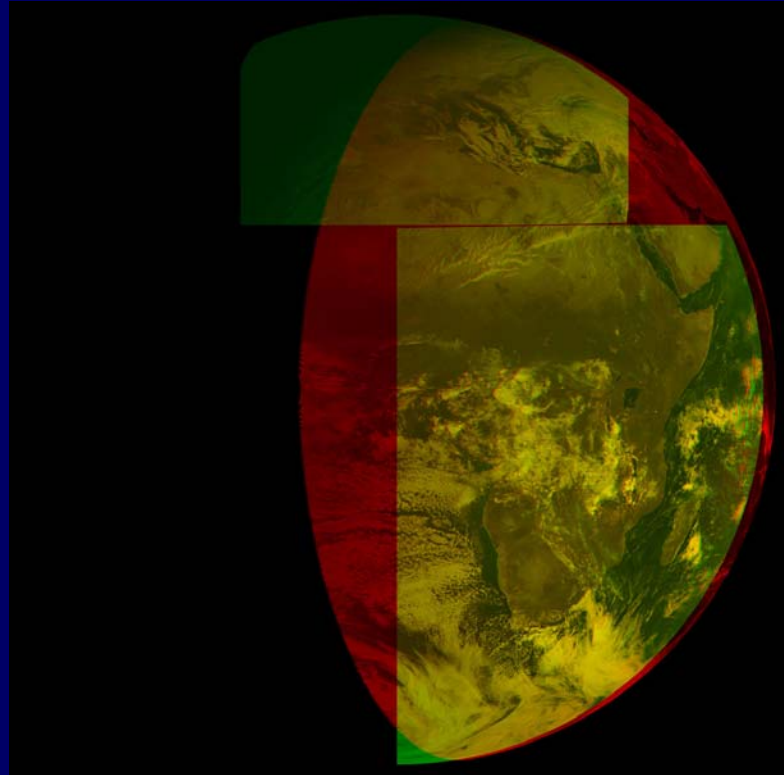
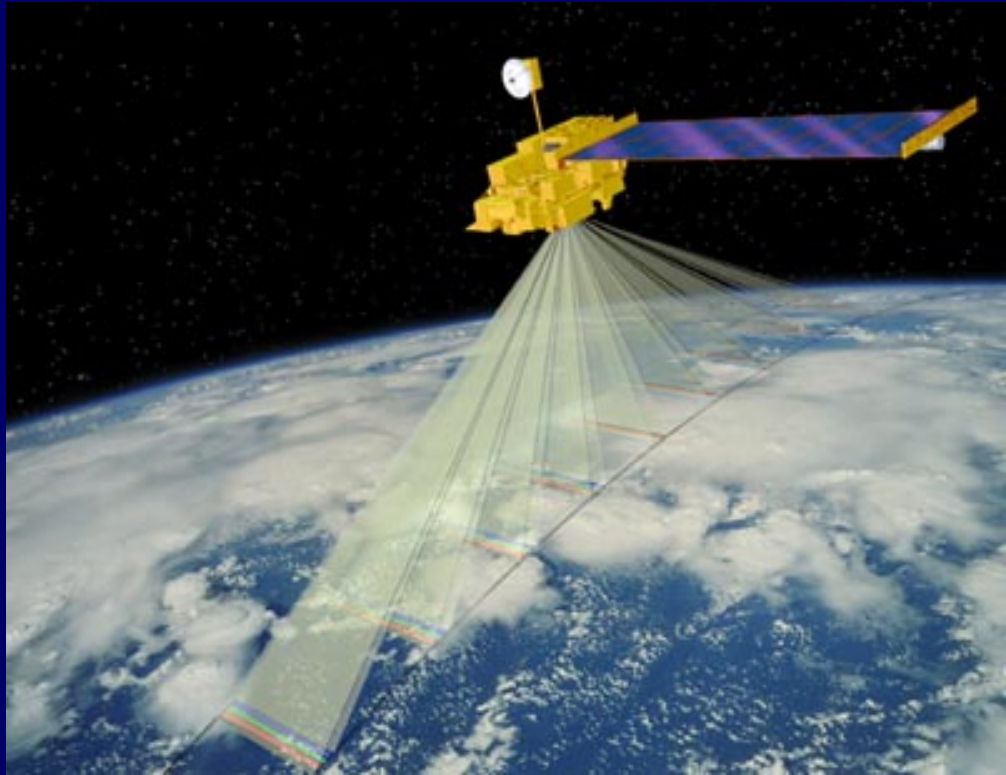


Multi-view photogrammetric analysis from satellite (focus on clouds)



Dr. Gabriela Seiz

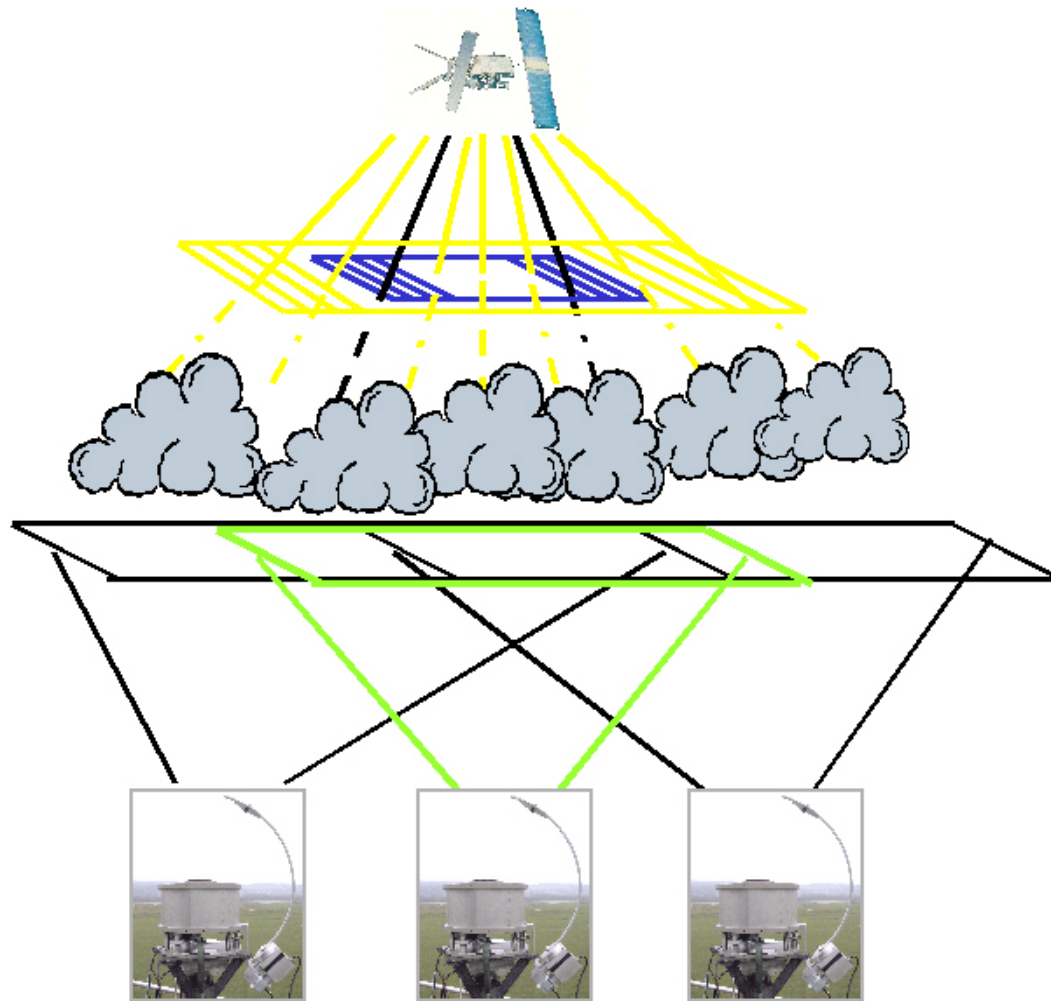
Acknowledgements

- EU-FP4 Project CLOUDMAP (1998-2001)
Partners: UCL (UK), FUB (D), DLR (D), KNMI (NL)
- EU-FP5 Project CLOUDMAP2 (2001-2004)
Partners: UCL, FUB, DLR, RAL (UK), KNMI, SMHI (S), MeteoSwiss
- EUMETSAT Cloud-top height comparison study (2003-2004)
Partners: FUB, RAL & Visiting Scientist, Eumetsat
- JPL, MISR Science Team, Visiting Scientist (2004)

Outline

- Introduction
- Polar-orbiting multi-view satellites
- Photogrammetric processing
- Case study MISR-ASTER-Meteosat6
- Geostationary satellites
- 3D cloud reconstruction with MISR and ASTER
- Conclusions
- Further examples of multi-view analysis with MISR

Introduction



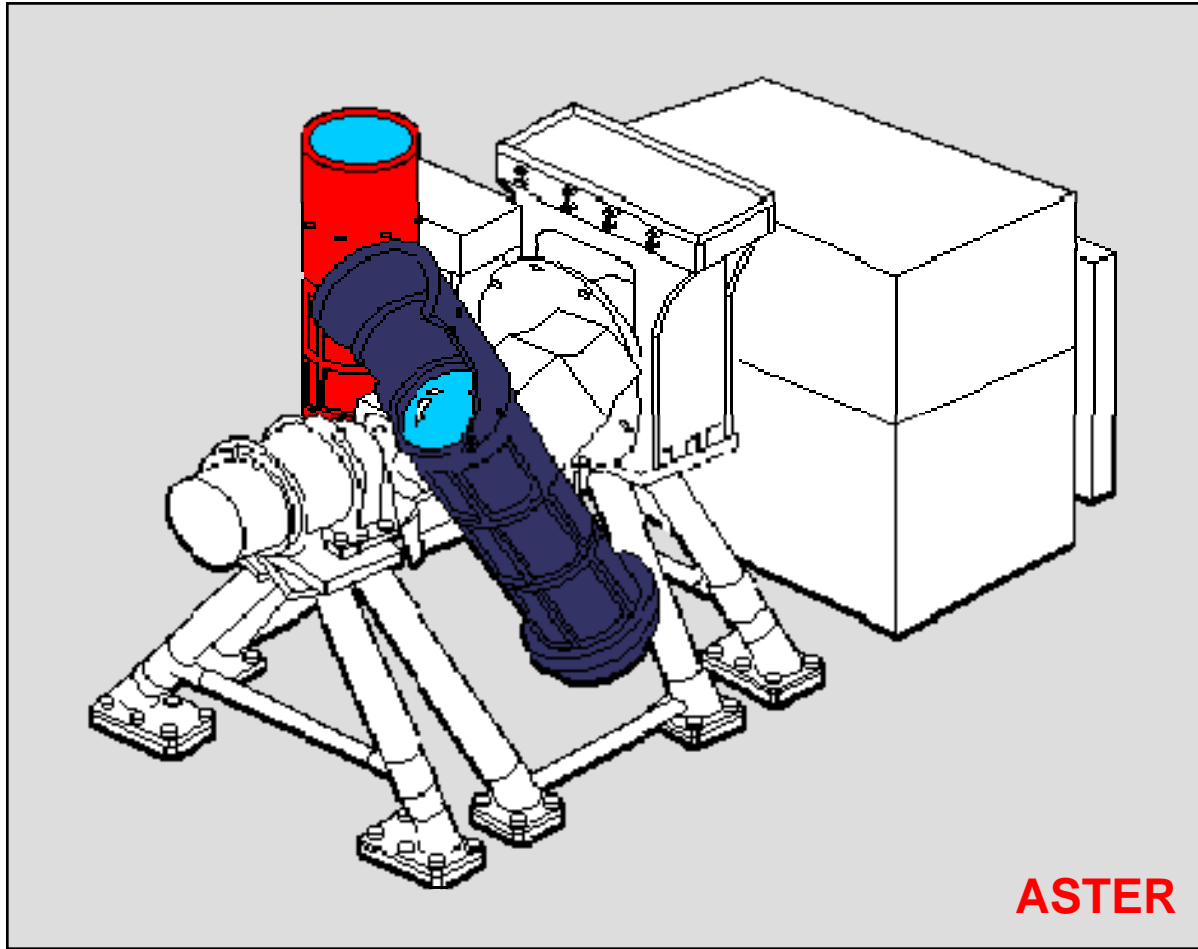
→ <http://www.photogrammetry.ethz.ch> (Prof. A. Gruen)

Polar-orbiting multi-view systems

	ATSR2, AATSR	MISR	ASTER
Platform	ERS-2, Envisat	EOS-Terra	EOS-Terra
Flying height [km]	780	705	705
System type	Scanning mirror (conical)	Linear CCD array	Linear CCD array
Data acquisition	Continuous	Continuous	On-demand
Viewing angles [°]	0.0, +55.0	0.0, ±26.1, ±45.6, ±60.0, ±70.5,	0.0, -27.6
Spatial resolution [m]	1000	275	15
Spectral channels [μm]	0.55, 0.67, 0.87, 1.6, 3.7, 10.8, 12.0	0.45, 0.55, 0.67, 0.87	0.82
Data product	GBT, ATS_TOA_1P	L1B2	L1B

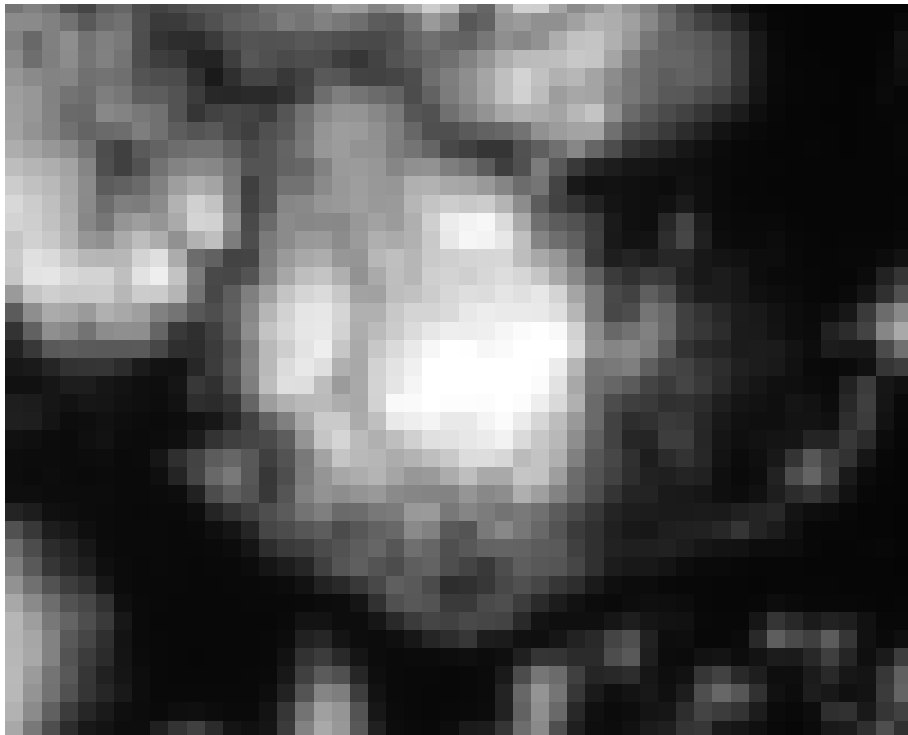
Polar-orbiting multi-view systems

- Data acquisition

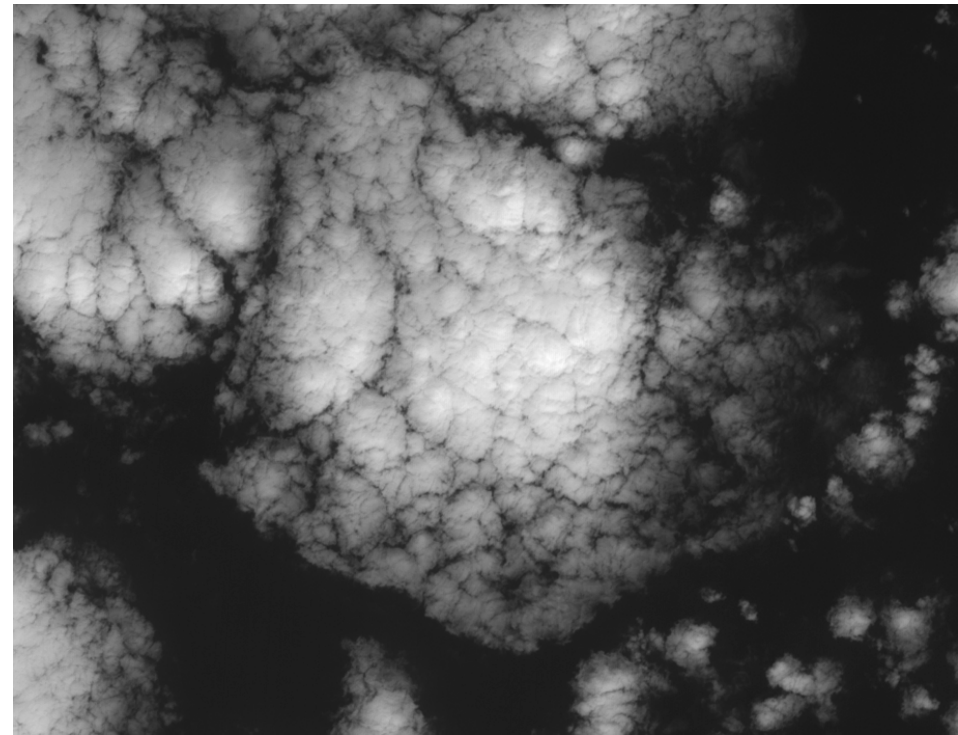


Polar-orbiting multi-view systems

- Spatial resolution

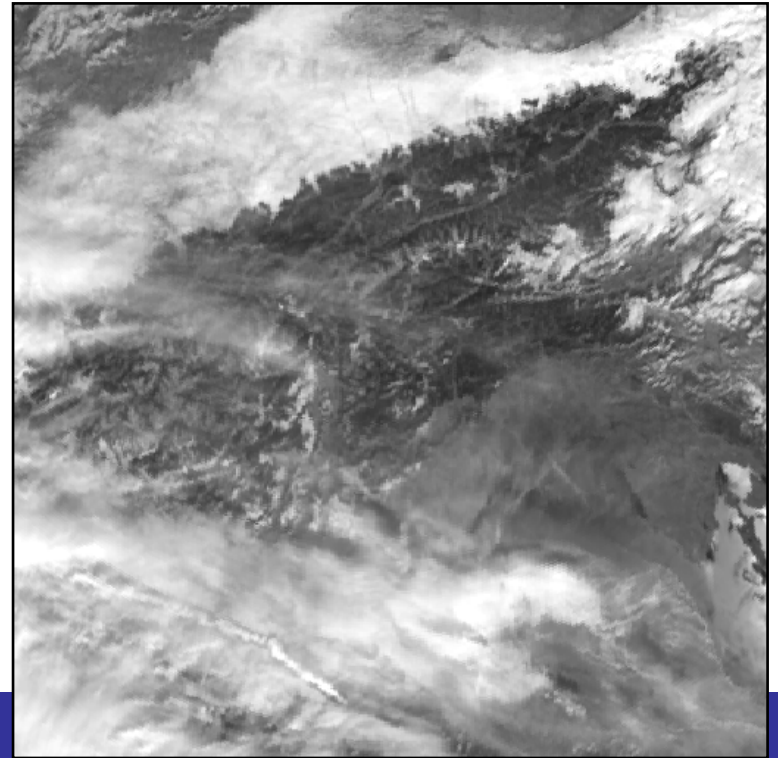
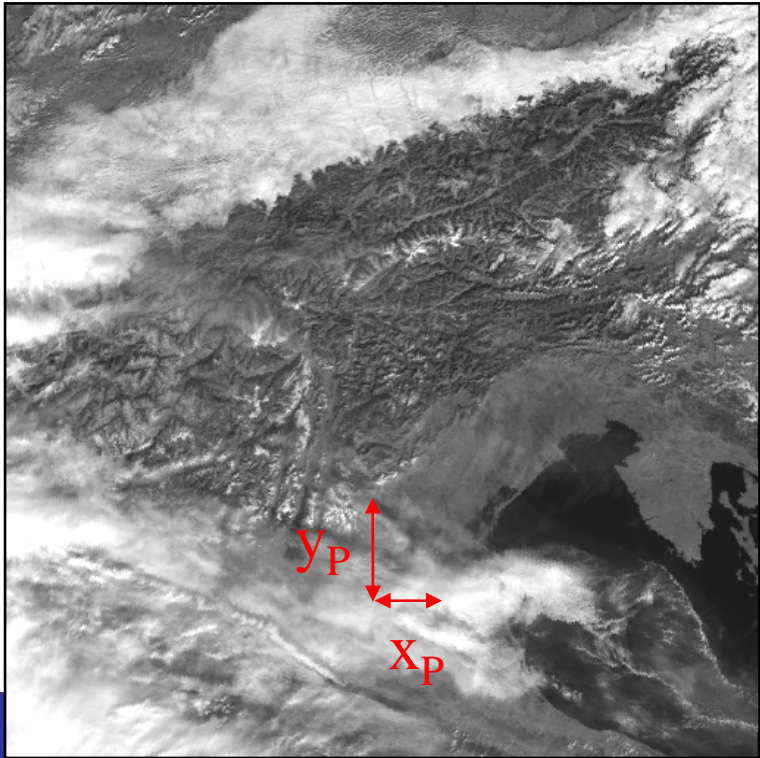


MISR An
(275 m)



ASTER 3N
(15 m)

Stereo CTH retrieval (polar-orbiting)

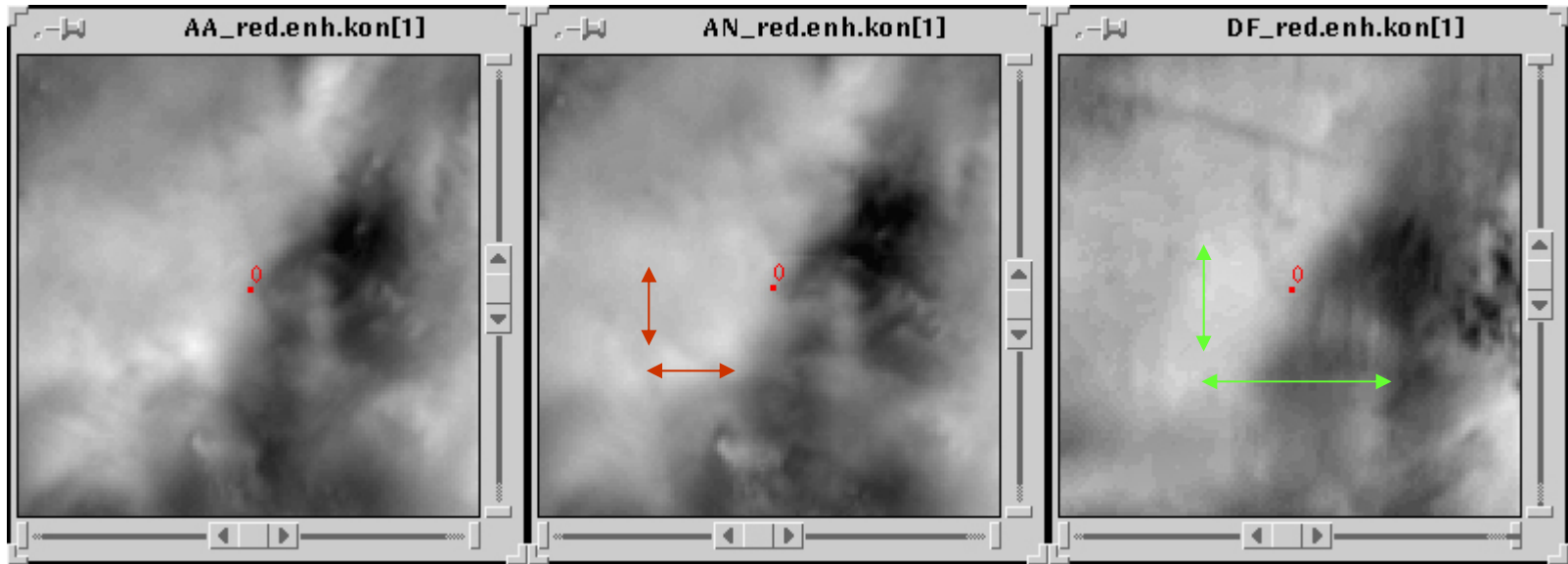


$x_P = f(\text{cross-track wind component})$

$y_P = f(\text{height, zenith angles, along-track wind component})$

(Lorenz, 1985)

Stereo CTH retrieval (polar-orbiting)



$$x_{dis12} = u(t_2 - t_1)$$

$$y_{dis12} = H(\tan \theta_1 - \tan \theta_2) + v(t_2 - t_1)$$

$\Rightarrow H, u, v$

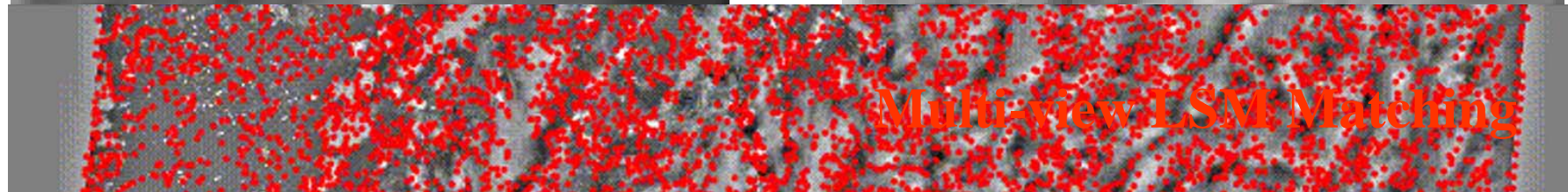
$$x_{dis13} = u(t_3 - t_1)$$

$$y_{dis13} = H(\tan \theta_1 - \tan \theta_3) + v(t_3 - t_1)$$

(Horváth and Davies, 2001)

Processing

Preprocessing



template

AN_red,enh,kon

patch_1

AA_red,enh,kon

patch_2

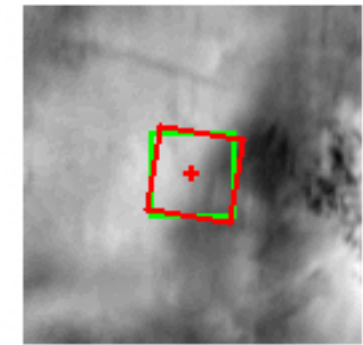
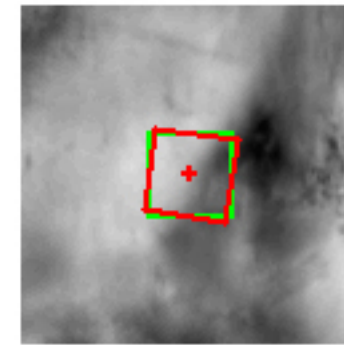
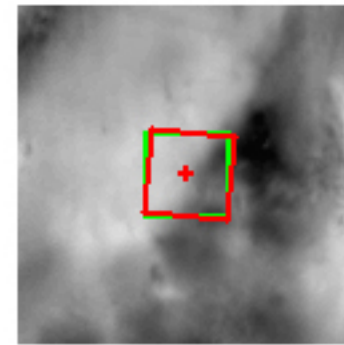
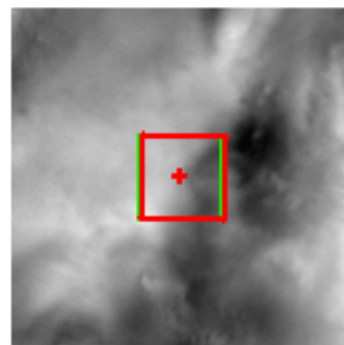
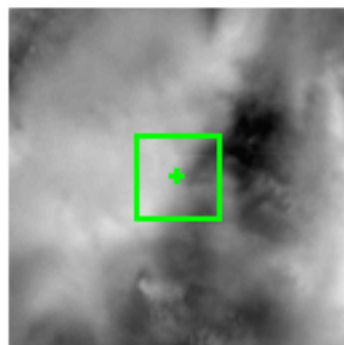
BF_red,enh,kon

patch_3

CF_red,enh,kon

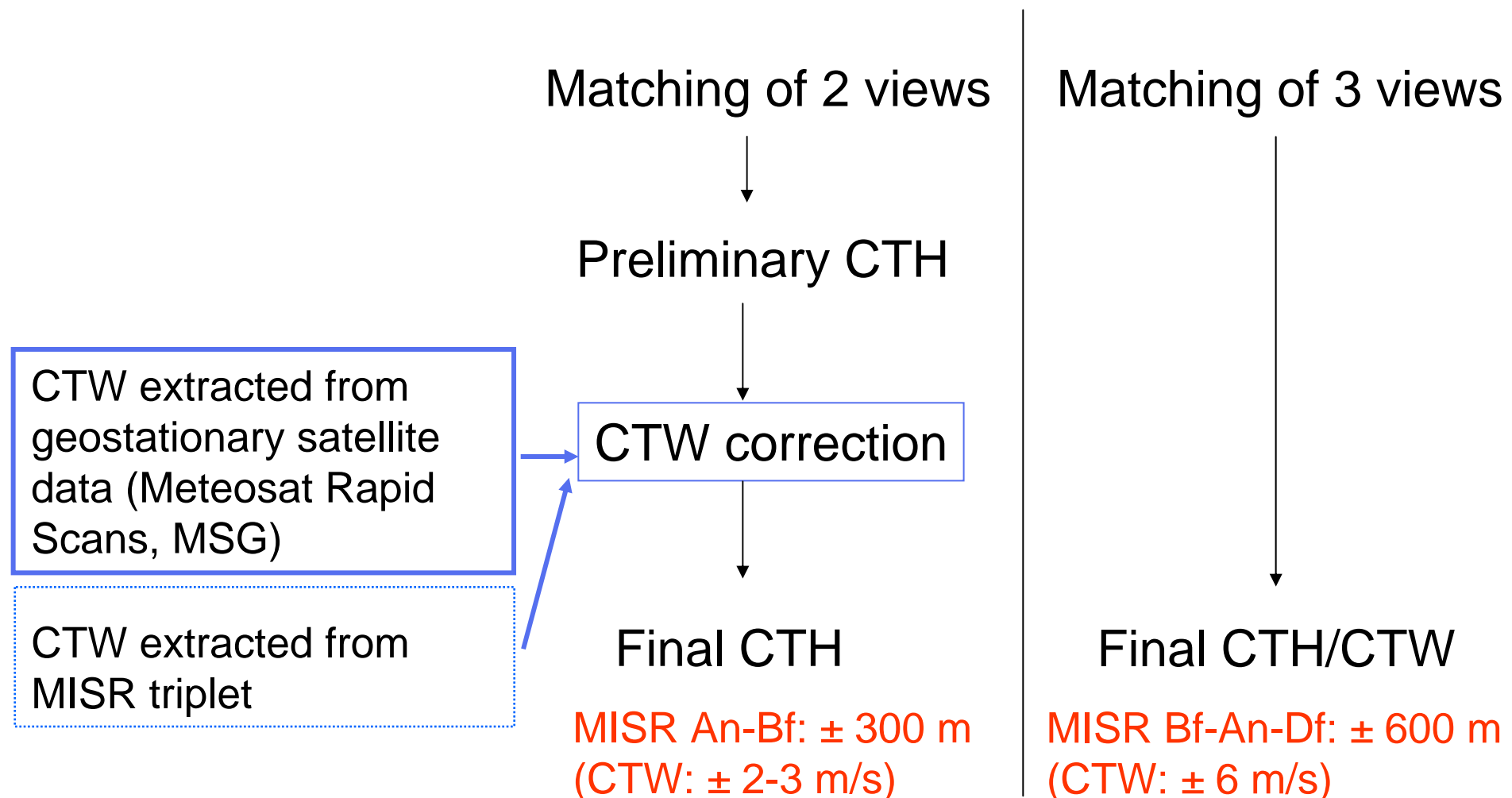
patch_4

DF_red,enh,kon



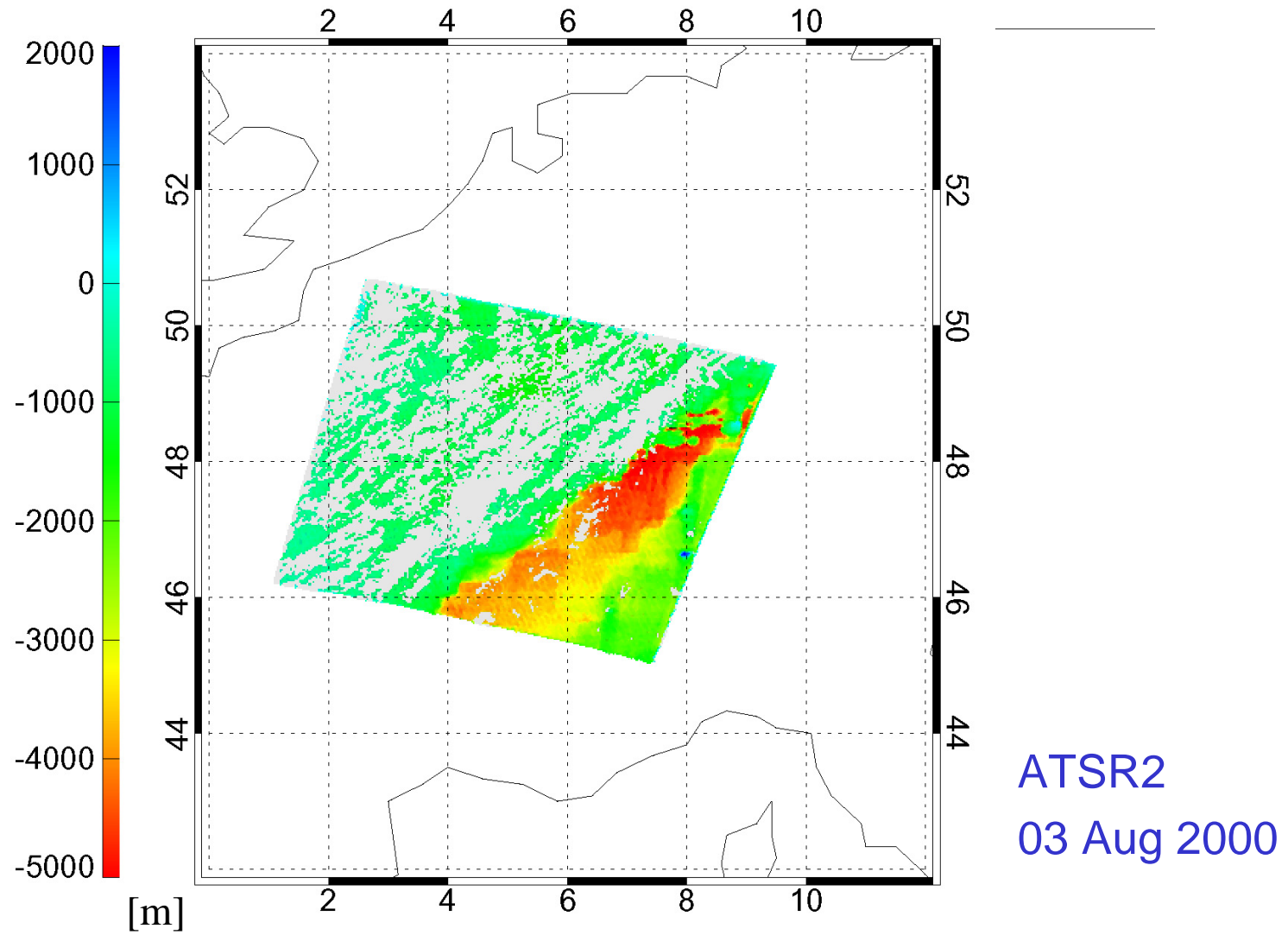
(Seiz, 2003)

Stereo CTH retrieval (polar-orbiting)

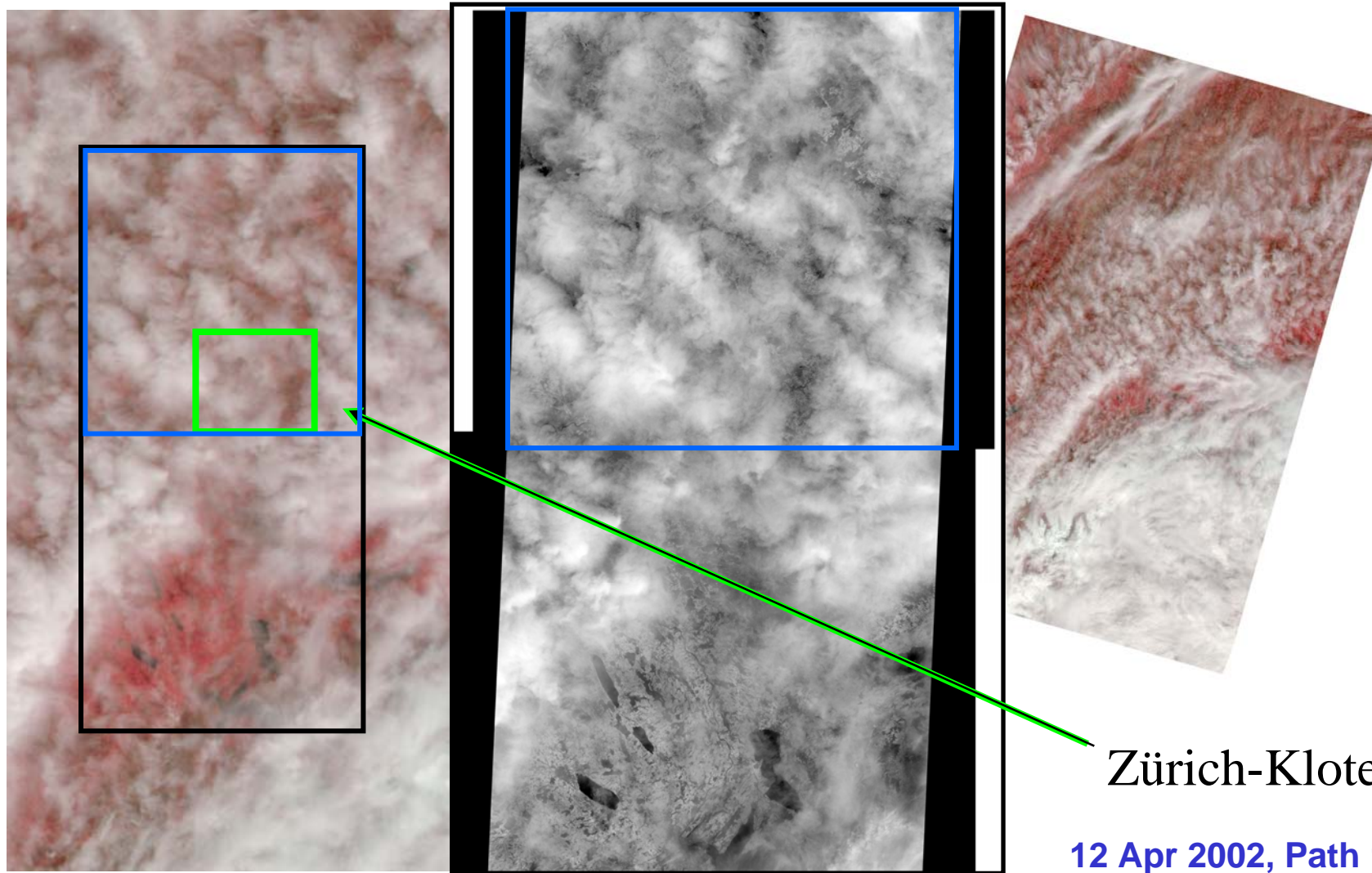


(Seiz, 2003)

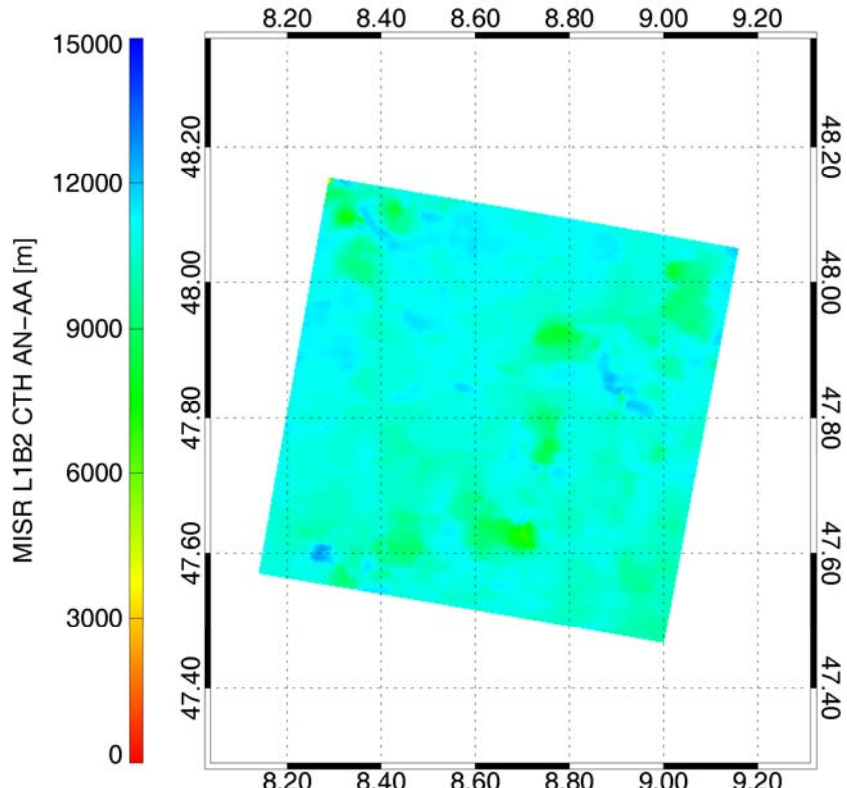
Cloud-top wind (CTW) correction



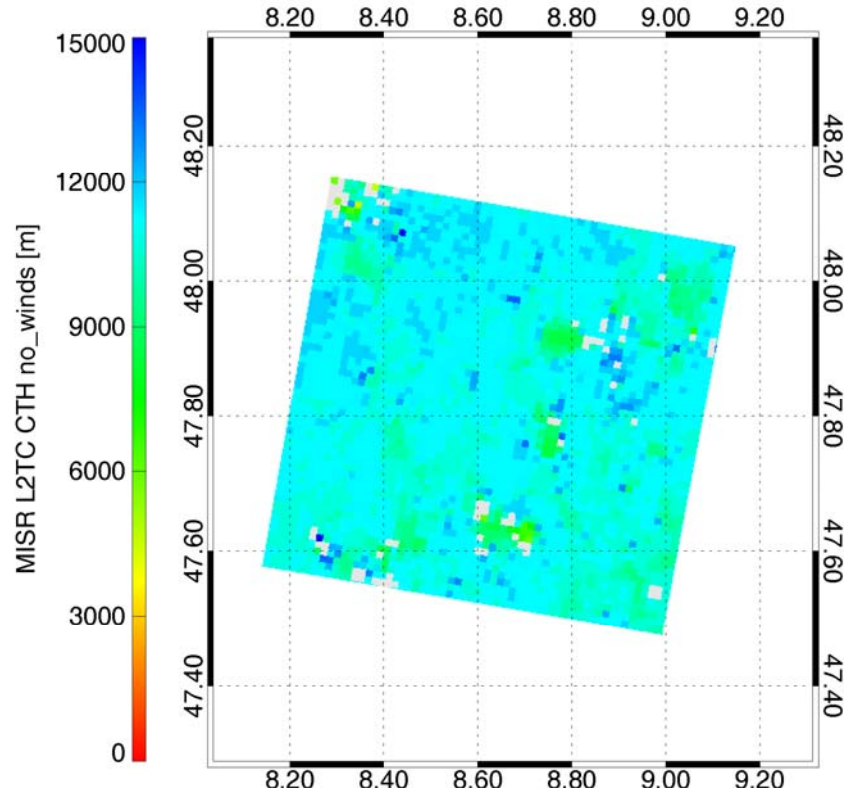
Case study: ASTER - MISR - Meteosat-6



Validation: MISR vs. ASTER CTH



MISR L1B2 CTH, An-Aa

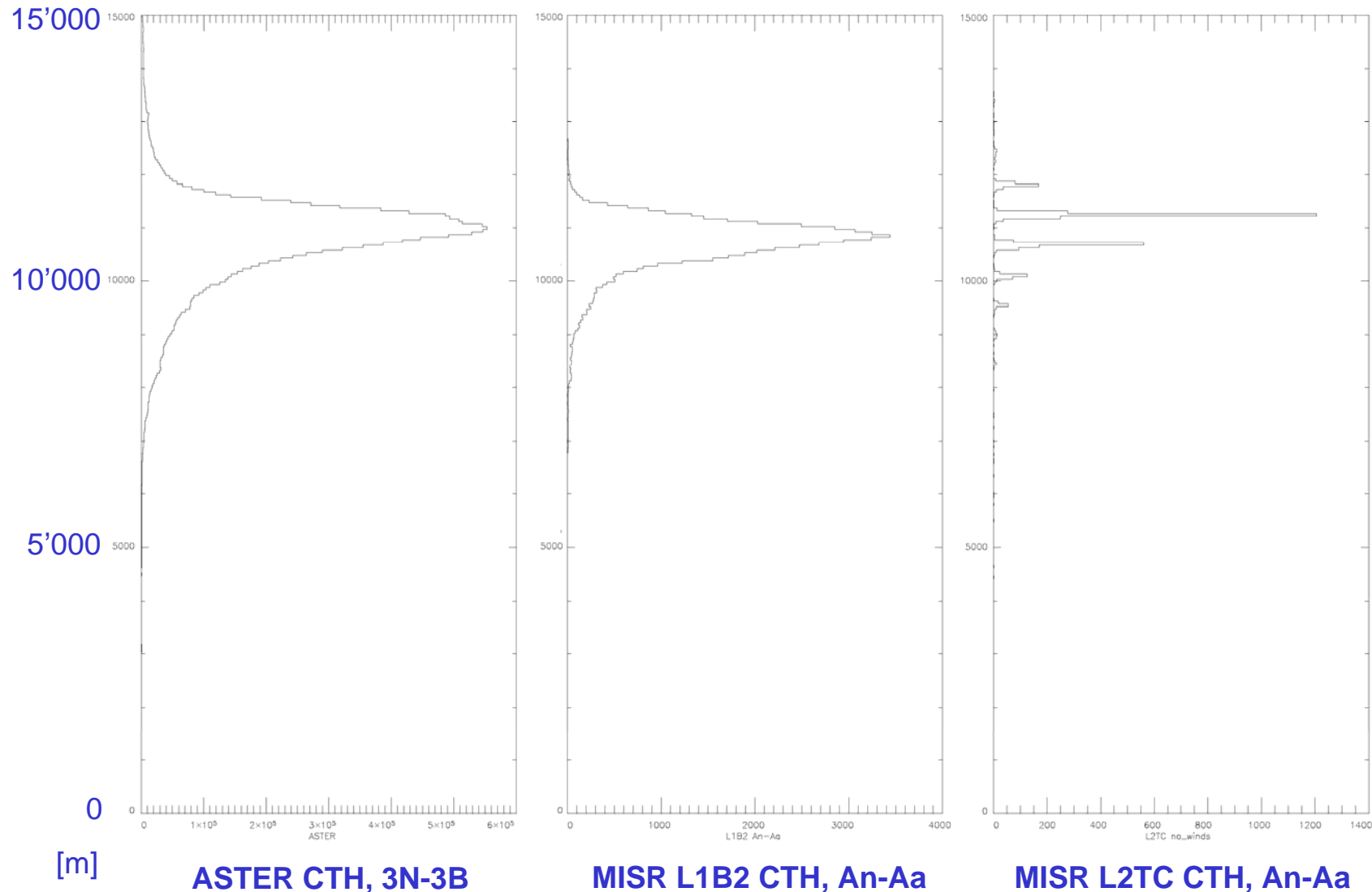


MISR L2TC CTH, An-Af/An-Aa

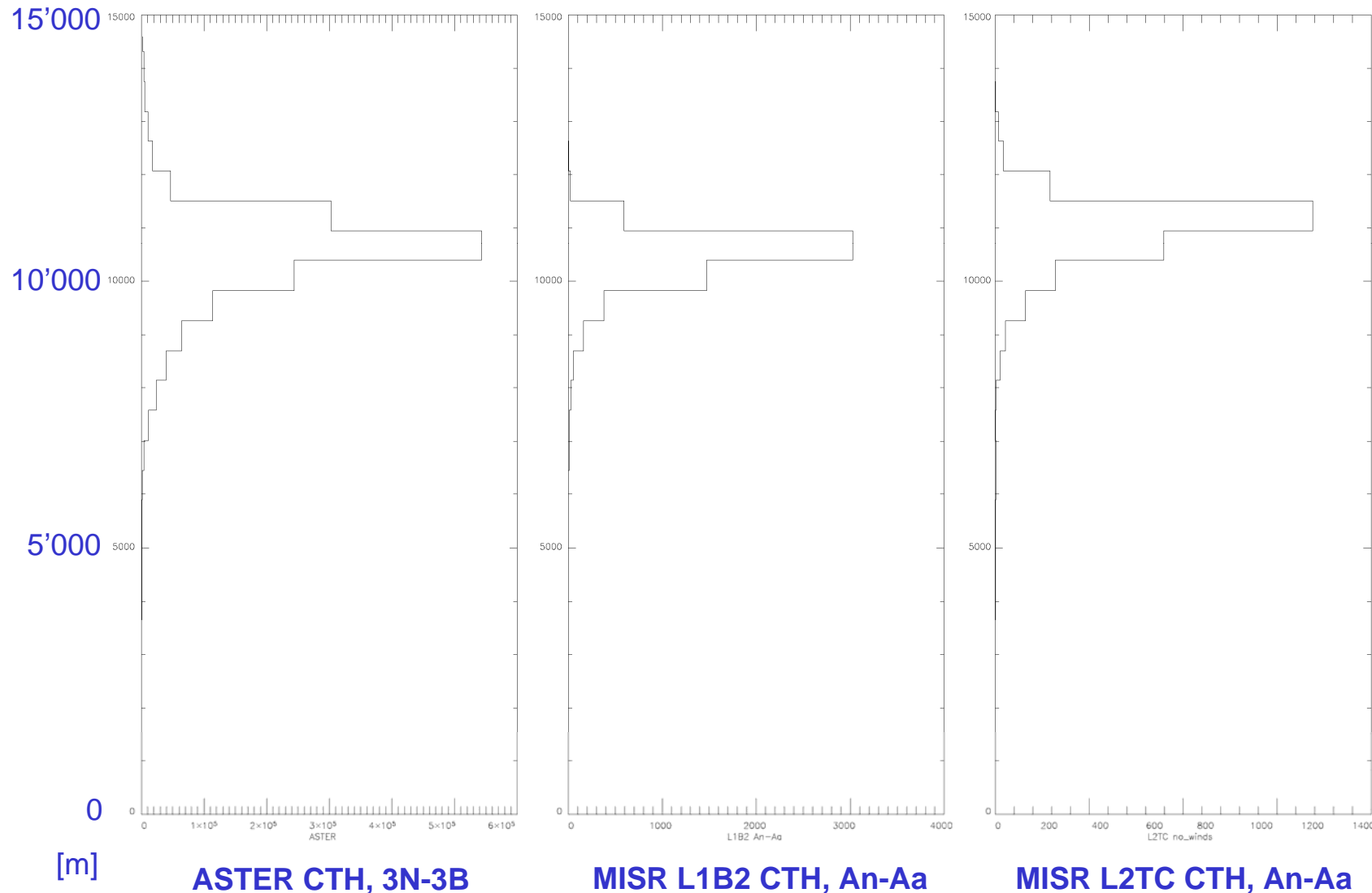
- MISR L1B2, ASTER L1B data
- Hierarchical LSM matching

(Seiz et al., IJRS, 2006)

Validation: MISR vs. ASTER CTH



Validation: MISR vs. ASTER CTH

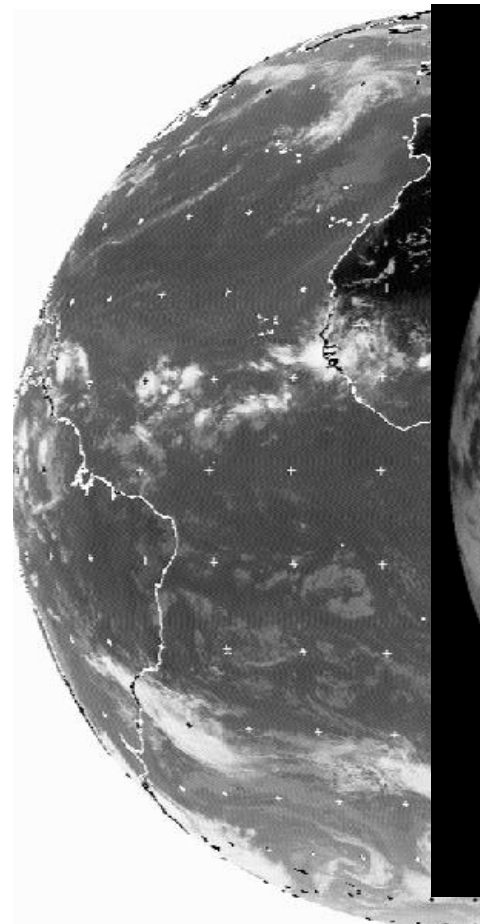


Stereo configurations

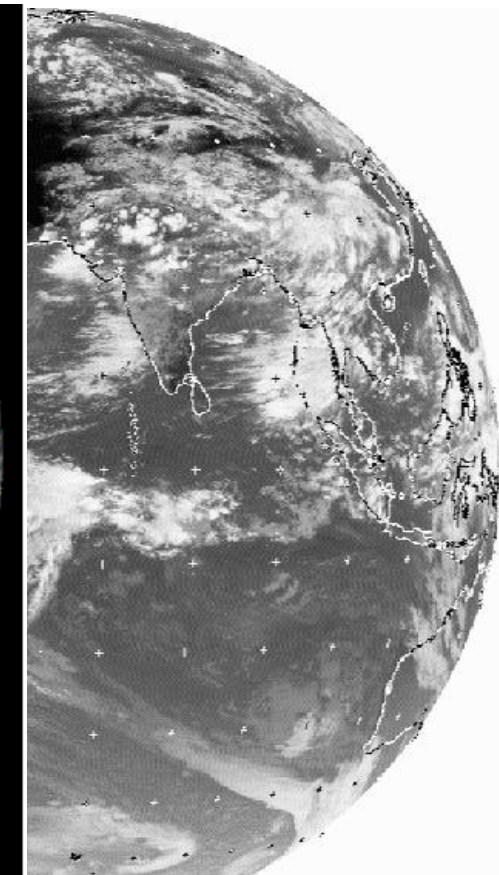
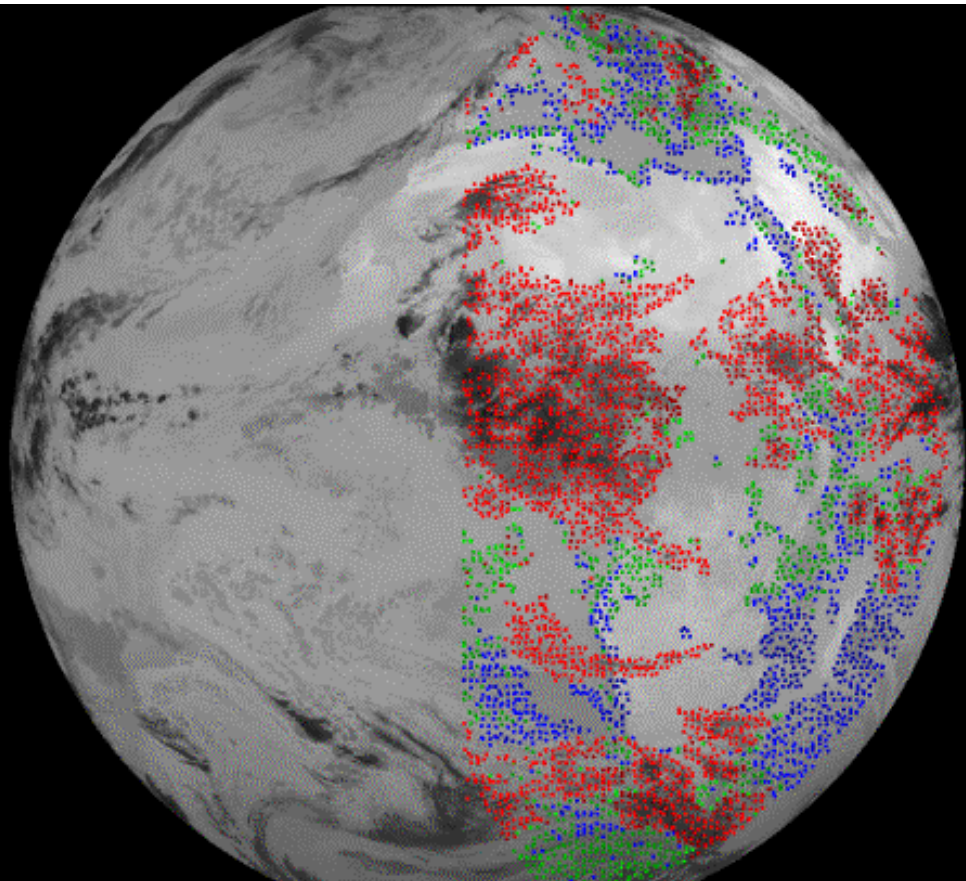
Sensor	B/H ratio	Δt [s]	Δh [m] for $\Delta y_p=0.5$ pixel	Δh [m] for $\Delta v'=3.0$ m/s	Δh_{total} [m]
AATSR	0.7-1.2	100-130	420-720	250-550	700
MISR AN_AF	0.49	45	280	275	400
MISR AN_BF	1.02	91	135	270	300
ASTER	0.6	55	13	275	276
Meteosat-6/-7	0.16	-	15'600	-	15'600
Meteosat-5/-7	1.5	-	1'020	-	1'020
Meteosat-5/-8	1.7				
Meteosat-8/-9					

Geostationary stereo: Meteosat satellites

Meteosat-7 (0°)



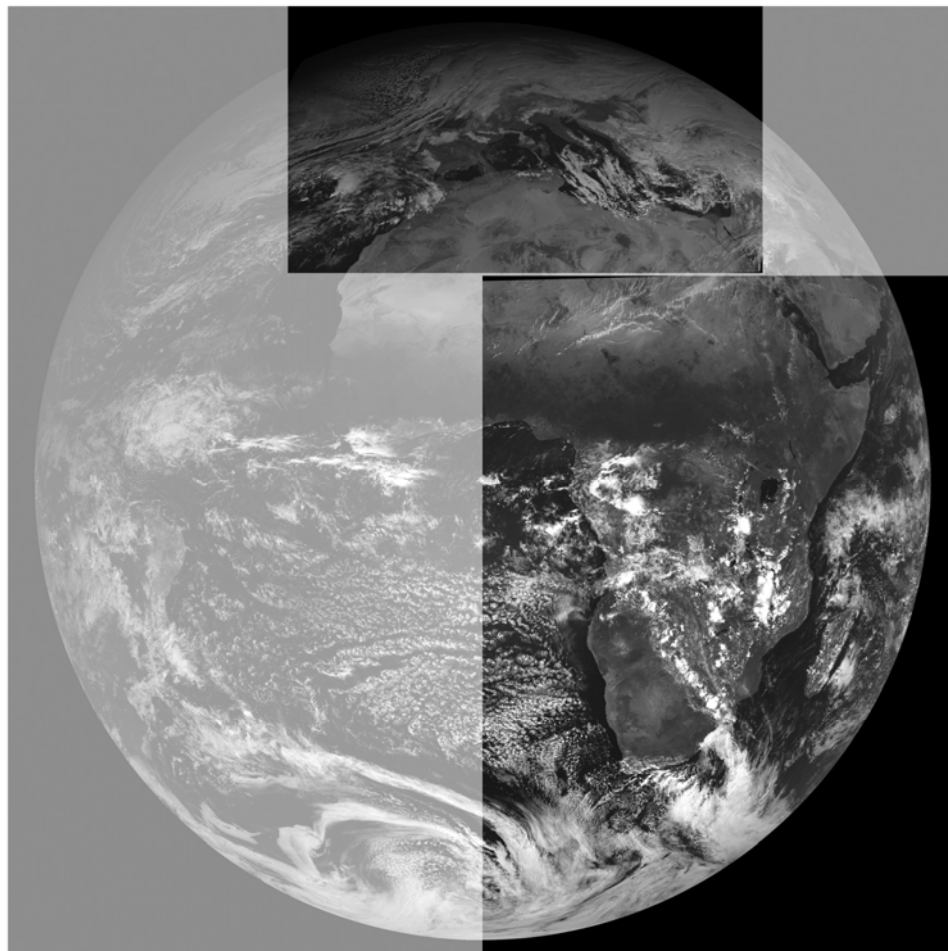
Meteosat-5 (63° E)



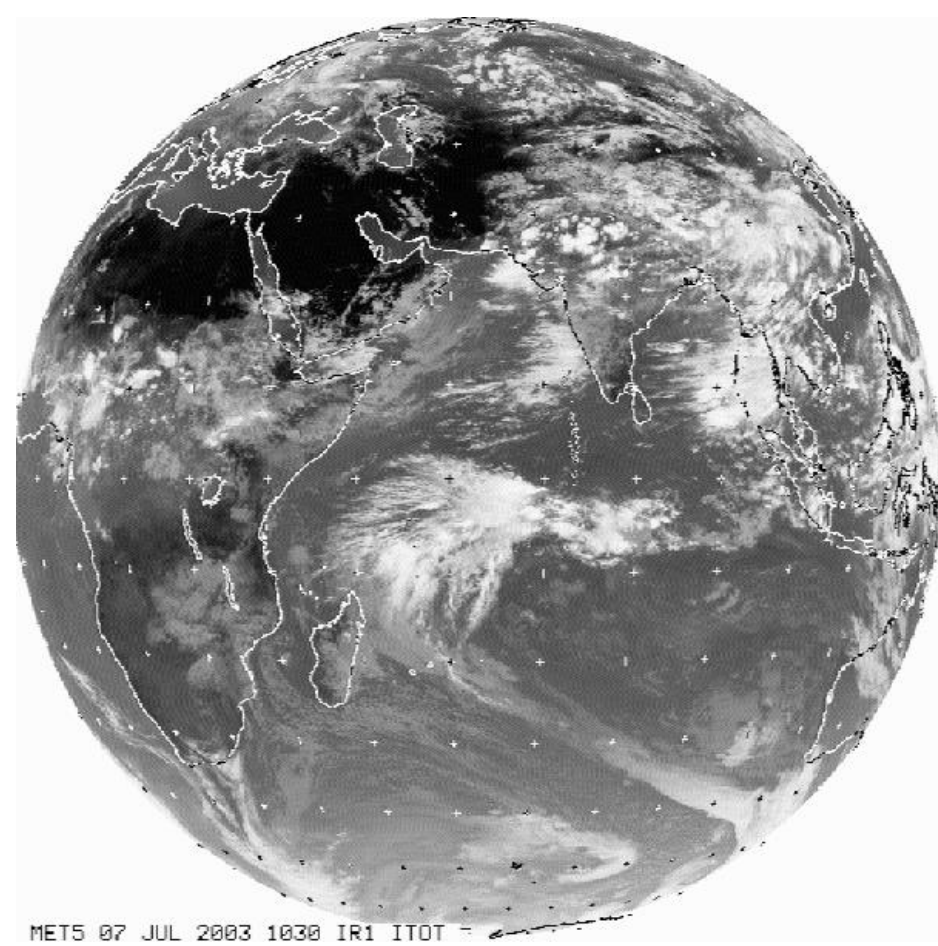
Wylie et al. (1998), Campbell and Holmlund (2004)

Geostationary stereo: Meteosat satellites

Meteosat-8 HRV (3.4° W, rectified to 0°)



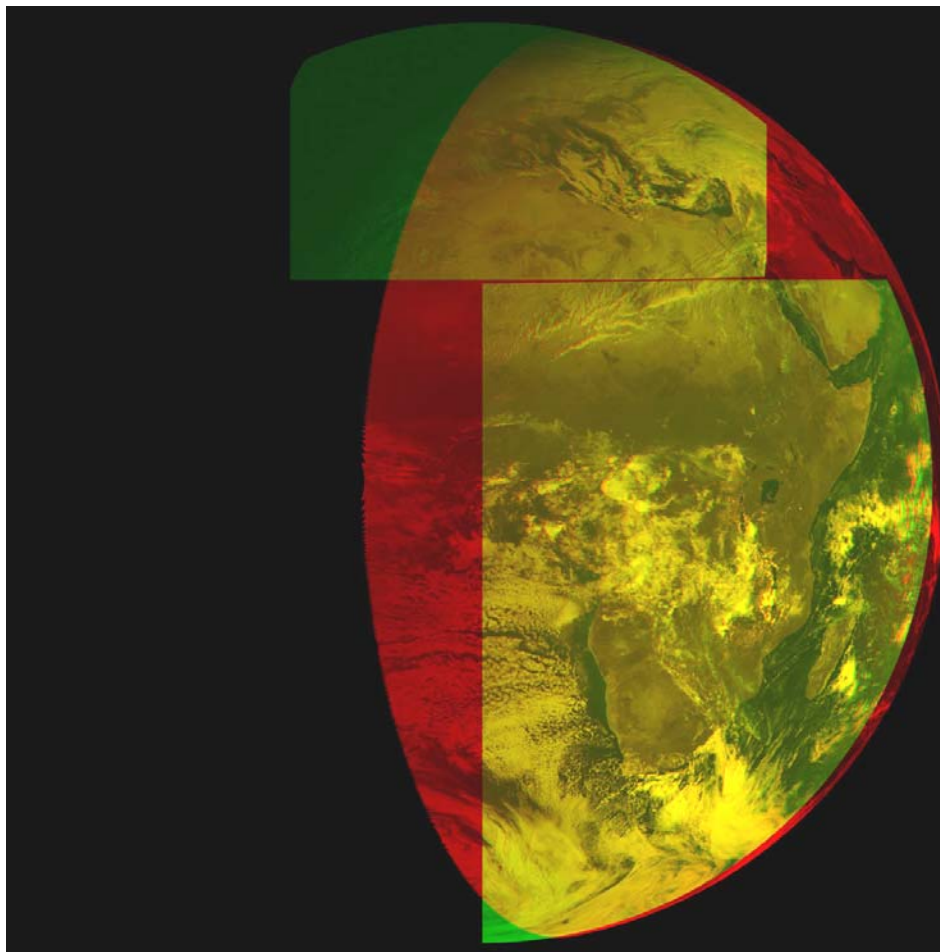
Meteosat-5 (63° E)



Geostationary stereo: Meteosat satellites

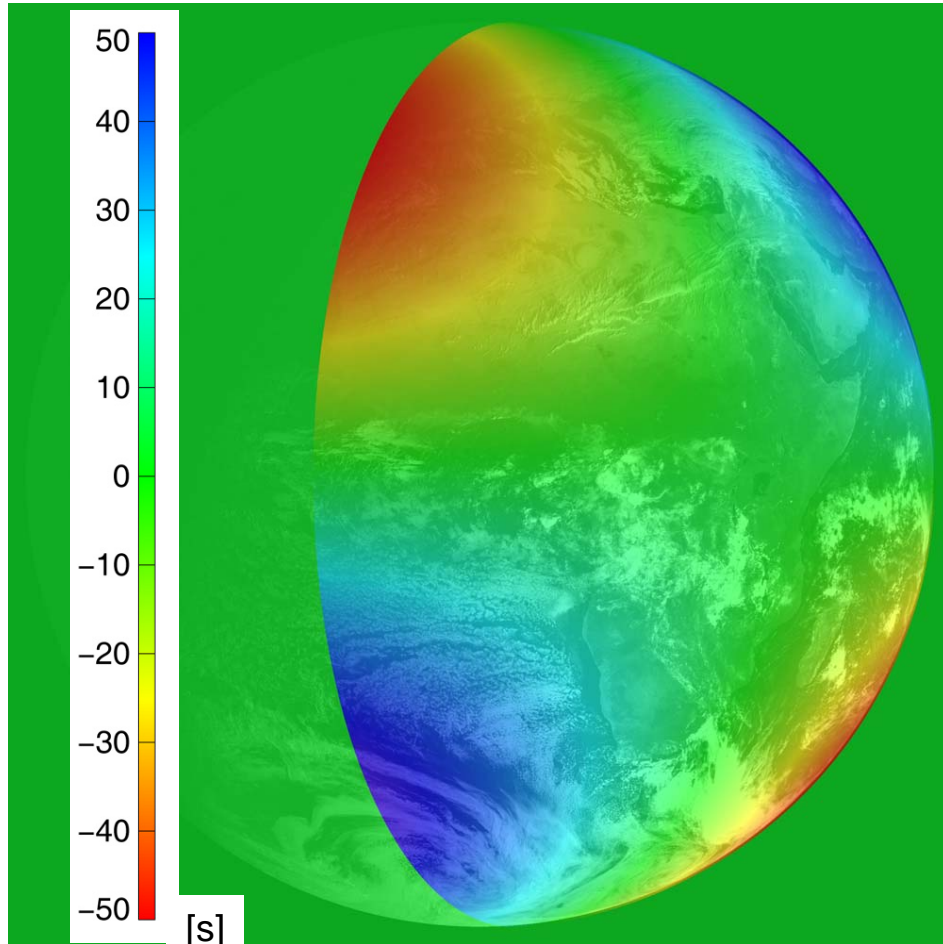
Meteosat-8 HRV (3.4° W, rectified to 0°)

Meteosat-5 (63° E)

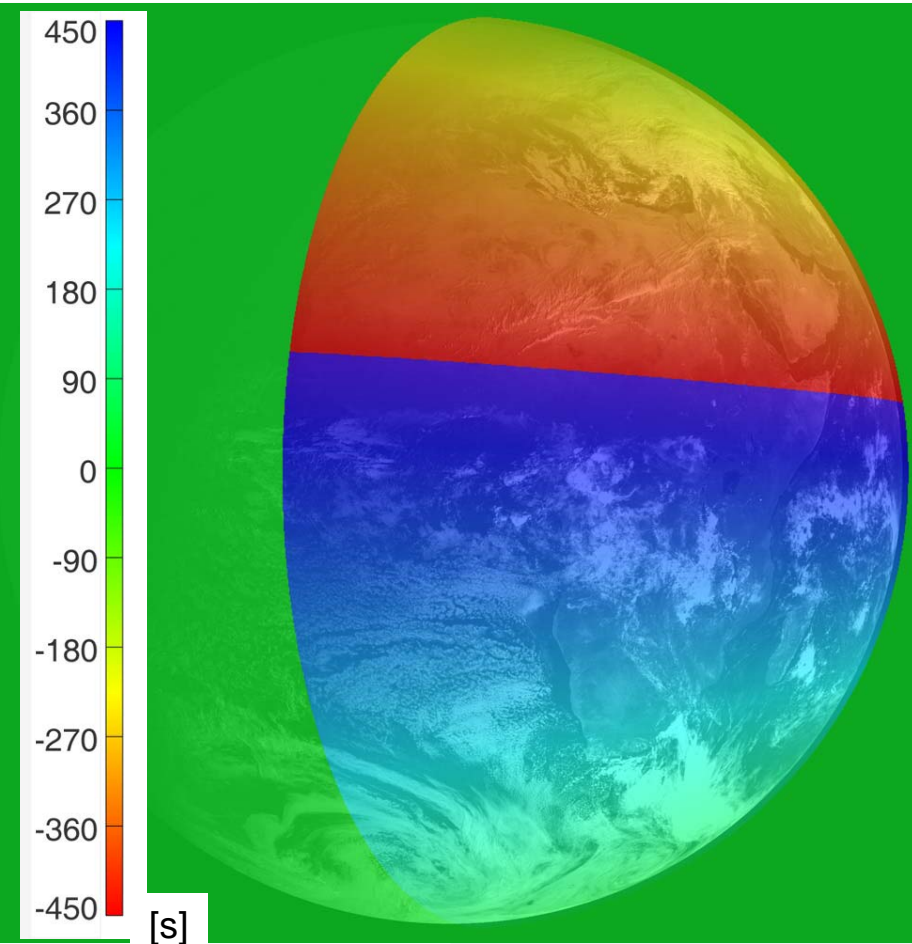


Geostationary stereo: Acquisition time

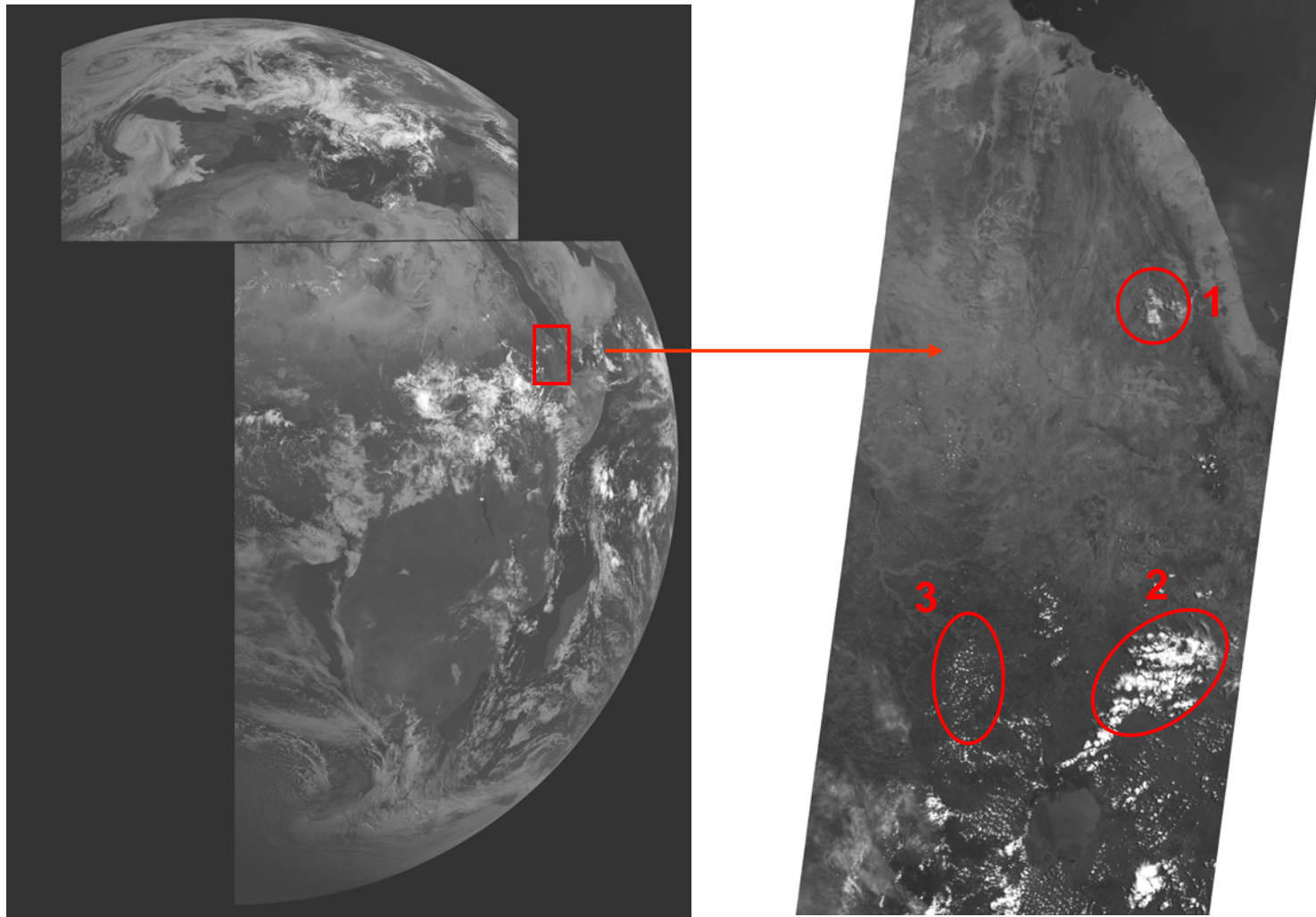
Meteosat-5 vs. Meteosat-7 (MFG)



Meteosat-5 vs. Meteosat-8 HRV (MSG)

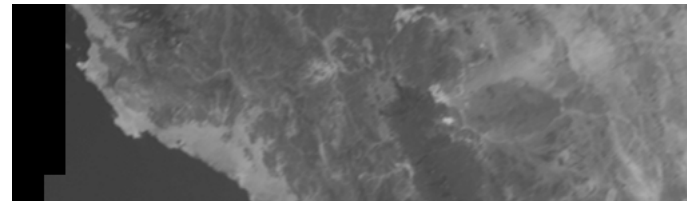
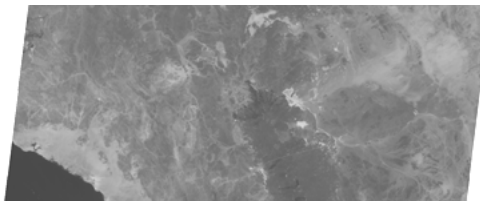


Geostationary stereo: Multi-view CTH retrieval



(5 June 2004, 08:00)

Geostationary stereo: Absolute geolocation



Sensor	dx	dy
Meteosat-5, 08:00 UTC	-2.10 ± 0.13	-3.54 ± 0.20
Meteosat-7, 08:00 UTC	0.39 ± 0.18	-0.94 ± 0.28
Meteosat-8, 08:00 UTC	-2.74 ± 0.09	-1.38 ± 0.18
Meteosat-8, 08:15 UTC	-3.15 ± 0.11	-1.19 ± 0.10

[MISR SOM pixels = 1.1 km]



MISR Path 170 (22.6 N | 37.6 E)

Geostationary stereo: Multi-view CTH retrieval

	M 5/M 7		M 5/M 8 HRV	
	CTH [m]	dist [m]	CTH [m]	dist [m]
Cloud1	6858 ± 177	716	6982 ± 245	277
Cloud2	6129 ± 215	218	6361 ± 311	404
Cloud3	2491 ± 274	233	2685 ± 457	482

after correction

	MISR L1B2 An-Aa CTH, wind_corr [m]	MISR L2TC CTH, best_winds [m]	MODIS MOD06 CTH, converted [m]
Cloud1	5931 ± 184	5954 ± 368	8949 ± 1851
Cloud2	5953 ± 254	6459 ± 400	7512 ± 753
Cloud3	2680 ± 105	2904 ± 396	975 ± 305

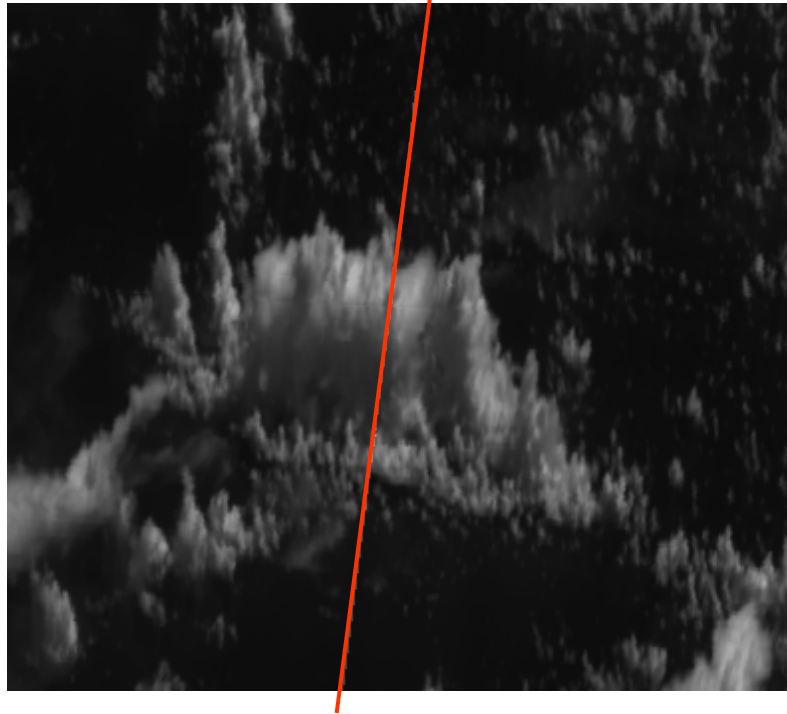
(Seiz and Tjemkes, JAMC, 2007)

Stereo configurations

Sensor	B/H ratio	Δt [s]	Δh [m] for $\Delta y_p=0.5$ pixel	Δh [m] for $\Delta v'=3.0$ m/s	Δh_{total} [m]
AATSR	0.7-1.2	100-130	420-720	250-550	700
MISR AN_AF	0.49	45	280	275	400
MISR AN_BF	1.02	91	135	270	300
ASTER	0.6	55	13	275	276
Meteosat-6/-7	0.16	-	15'600	-	15'600
Meteosat-5/-7	1.5	-	1'020	-	1'020
Meteosat-5/-8	1.7	390	620	700	940
Meteosat-8/-9	1.7	-	440	-	440

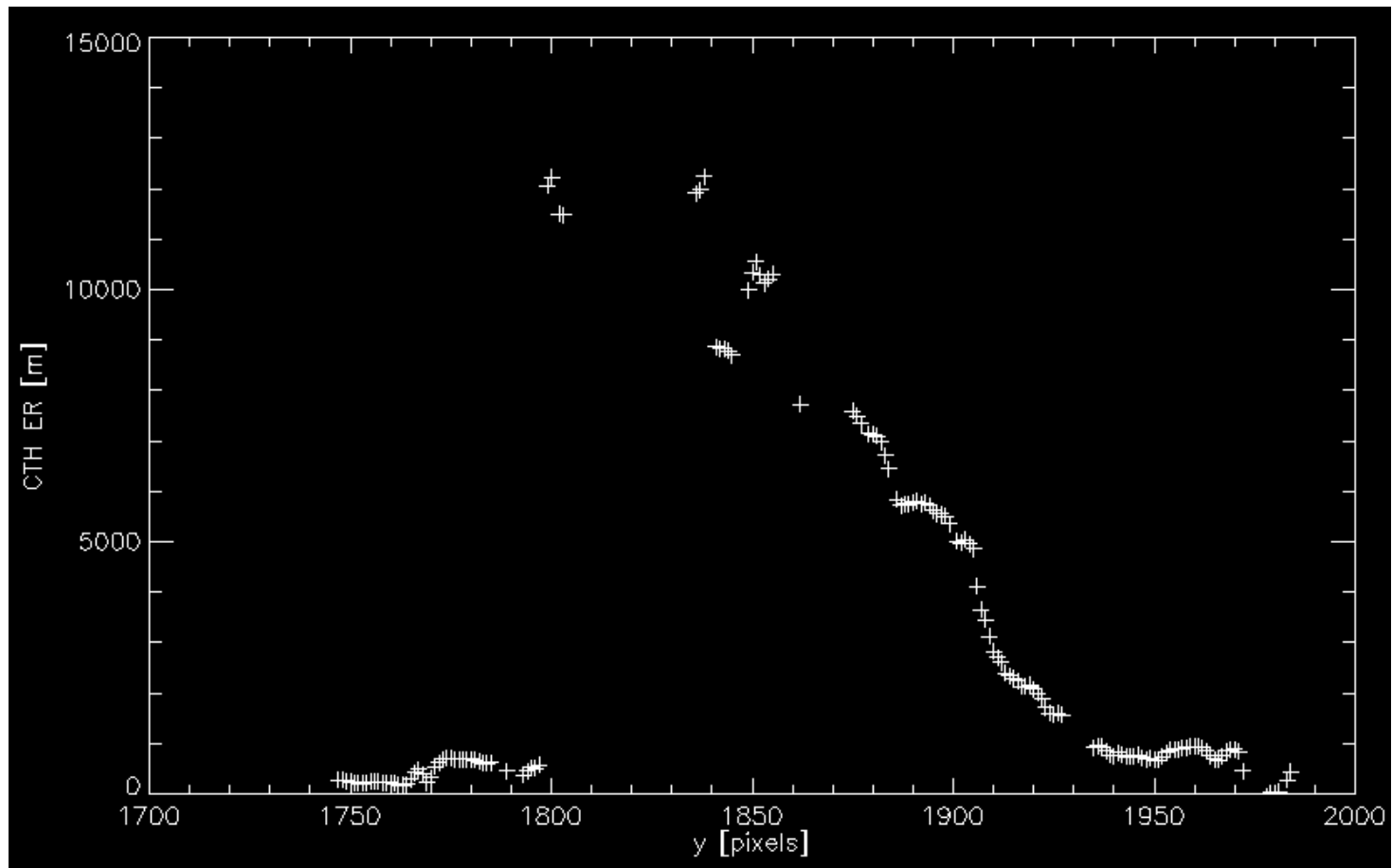
3D cloud reconstruction from MISR

Isolated convective cloud over ocean
(2 Sep 2003, Path 78, 22:15:07 UTC)



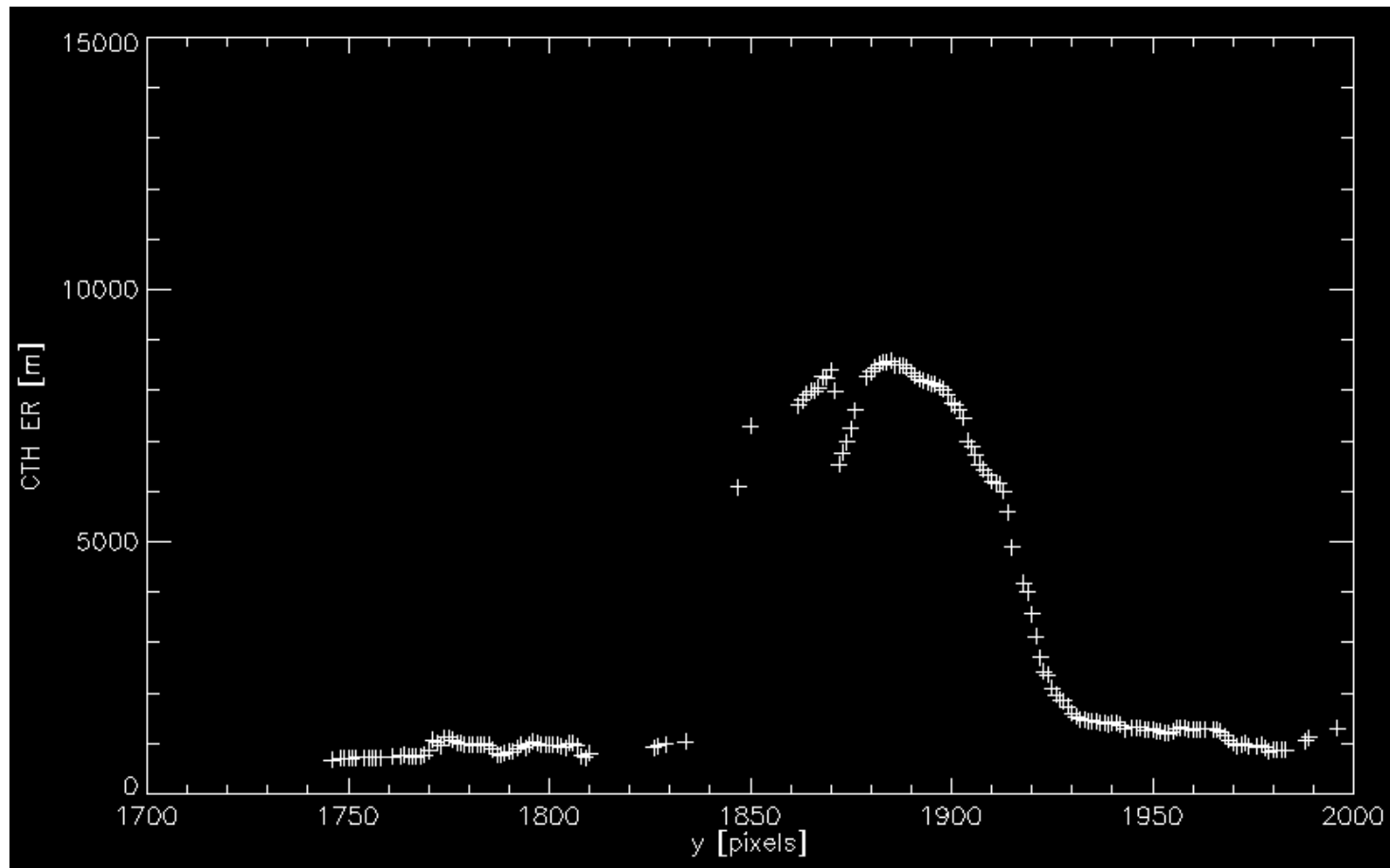
- LSM matching along line
- 8 camera combinations,
An-Af, Af-Bf, Bf-Cf, Cf-Df
An-Aa, Aa-Ba, Ba-Ca, Ca-Da

3D cloud reconstruction from MISR



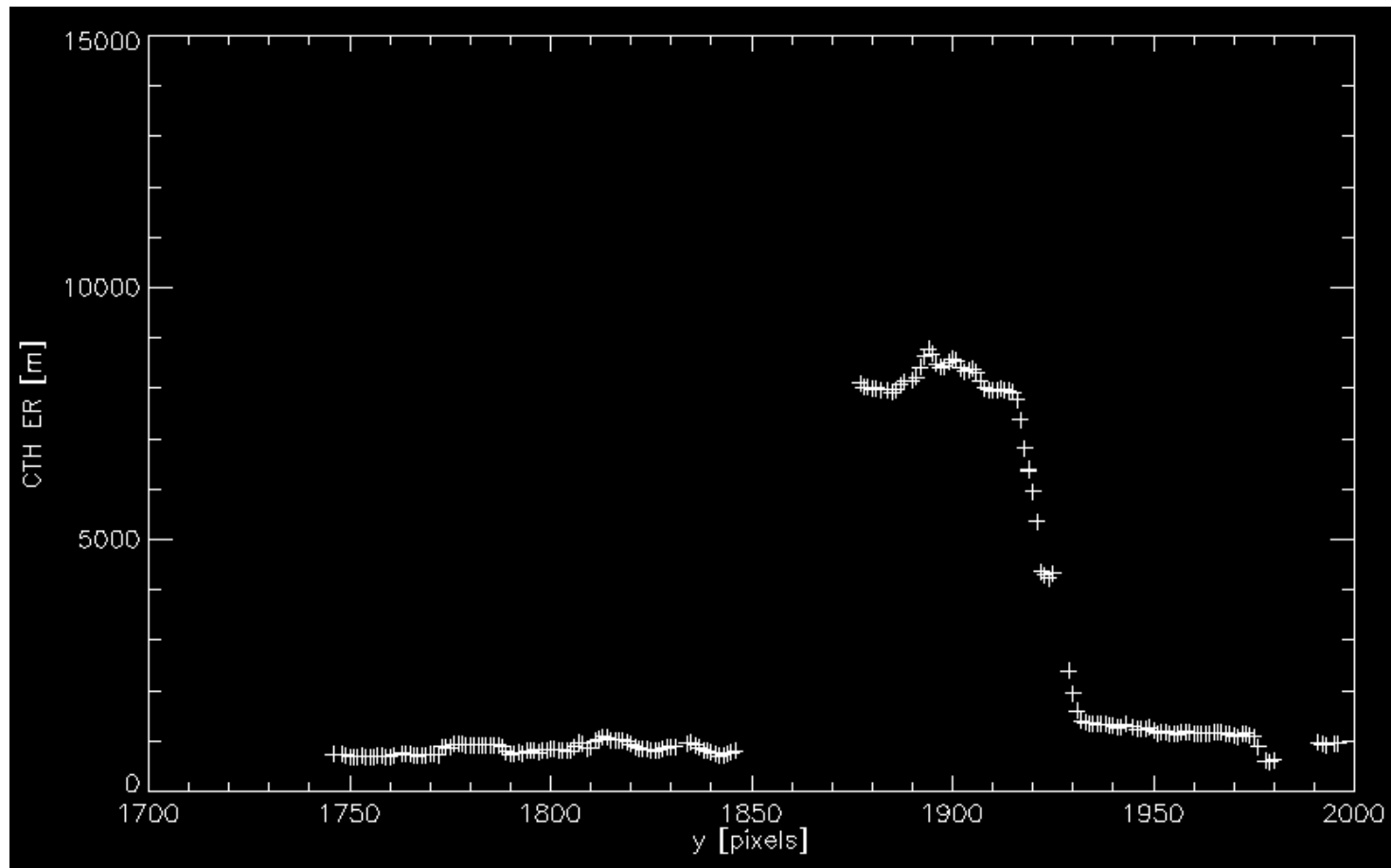
- Ca-Da

3D cloud reconstruction from MISR



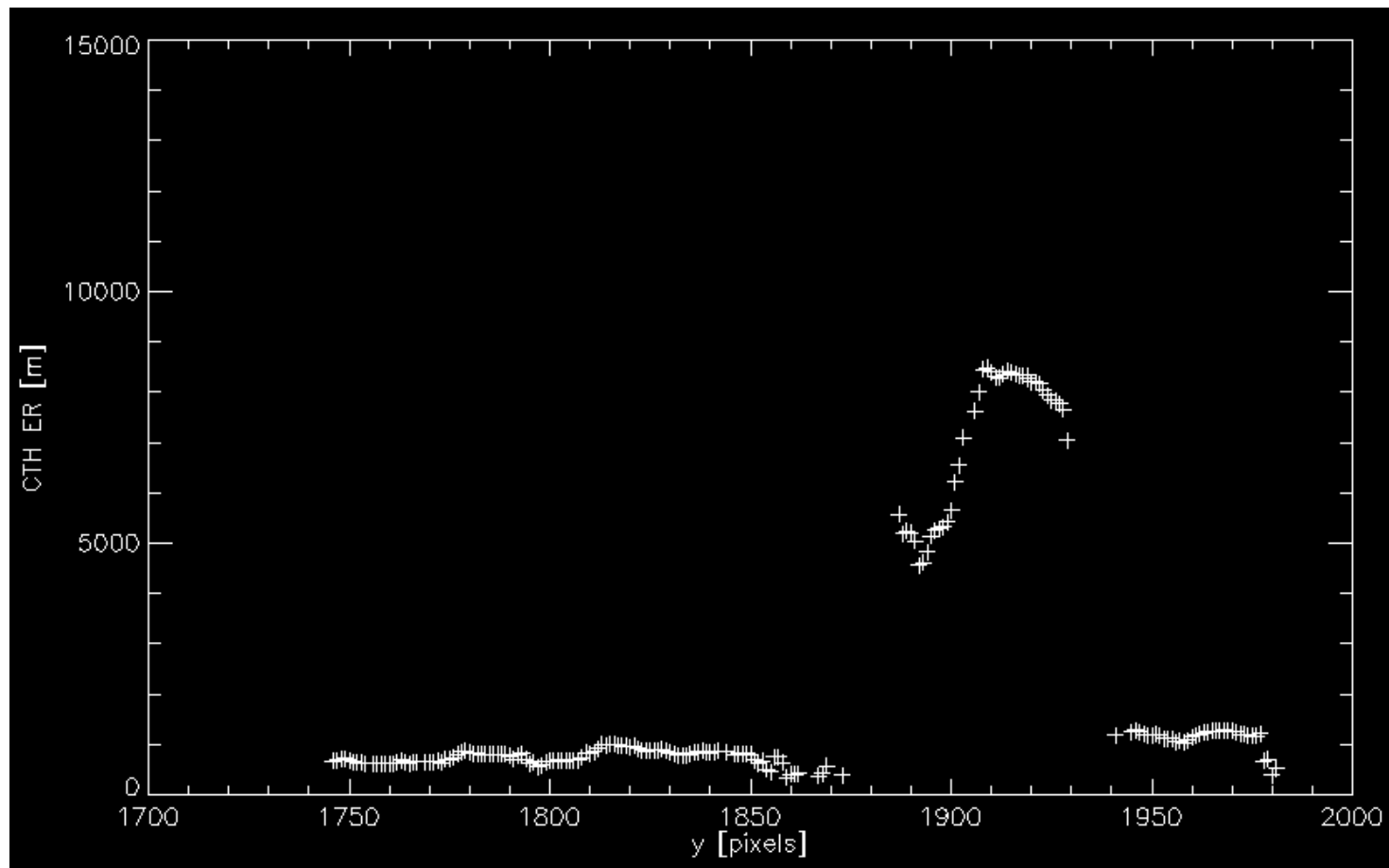
- Ba-Ca

3D cloud reconstruction from MISR



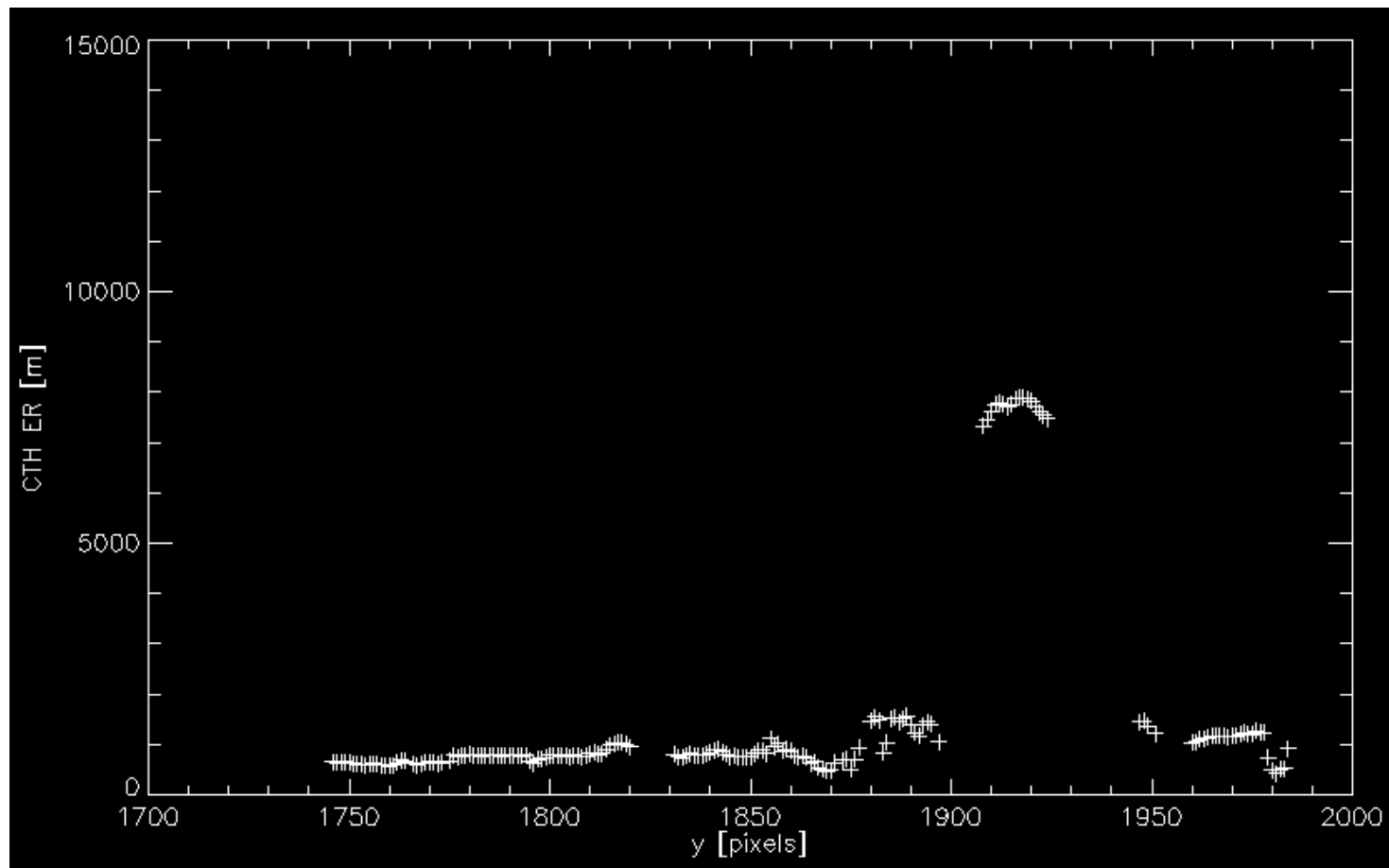
- Aa-Ba

3D cloud reconstruction from MISR



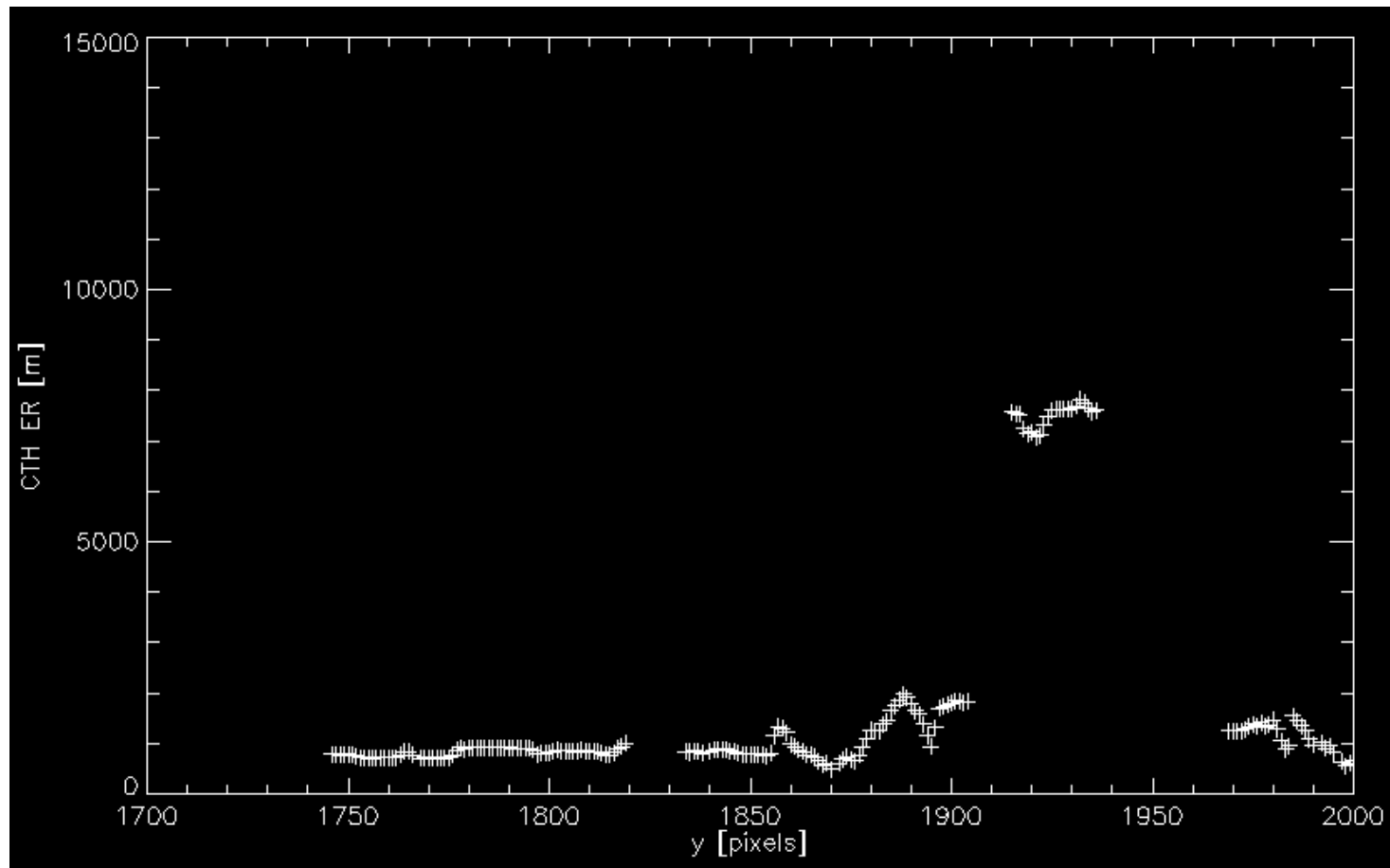
- An-Aa

3D cloud reconstruction from MISR



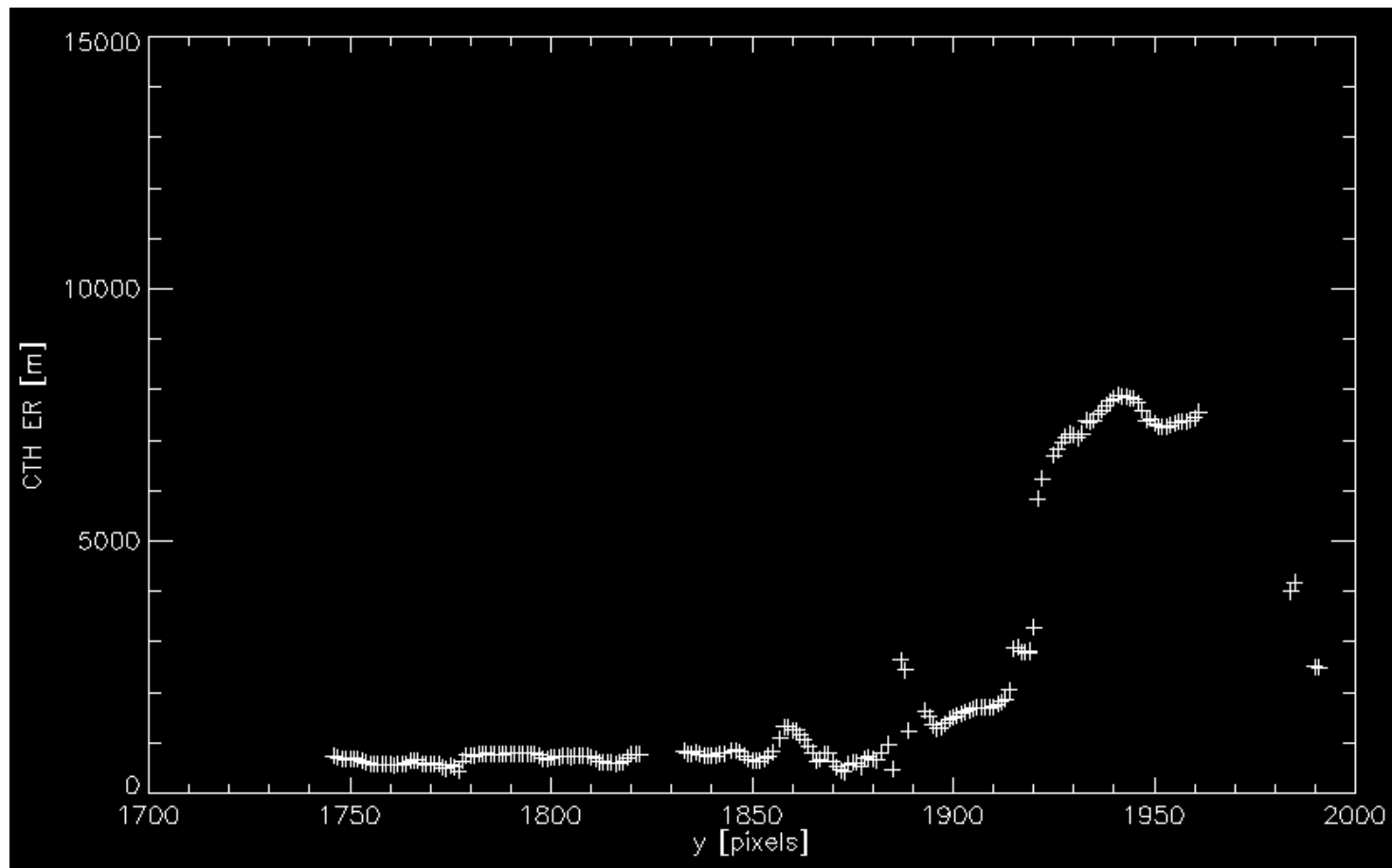
- An-Af

3D cloud reconstruction from MISR



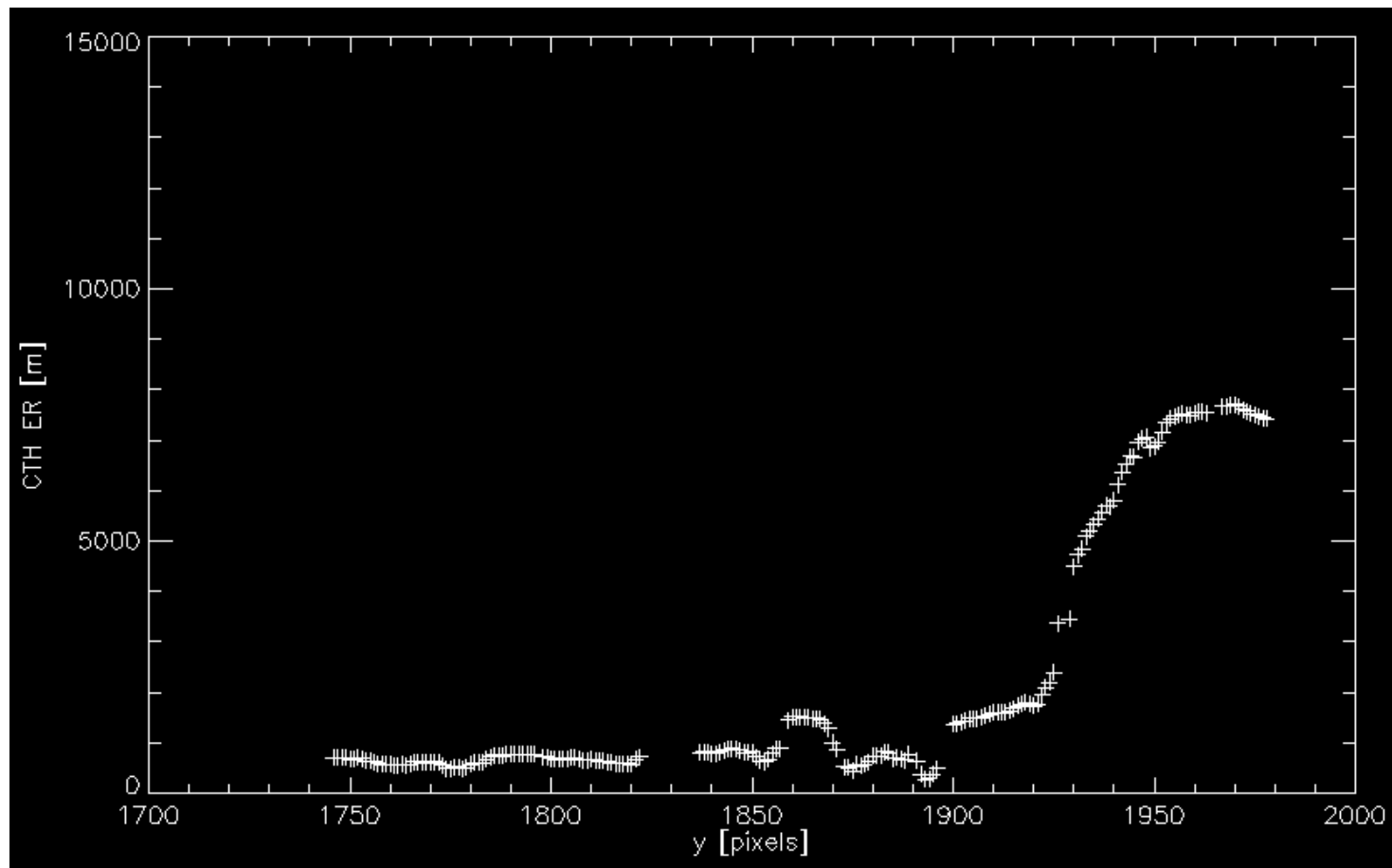
- Af-Bf

3D cloud reconstruction from MISR



- Bf-Cf

3D cloud reconstruction from MISR

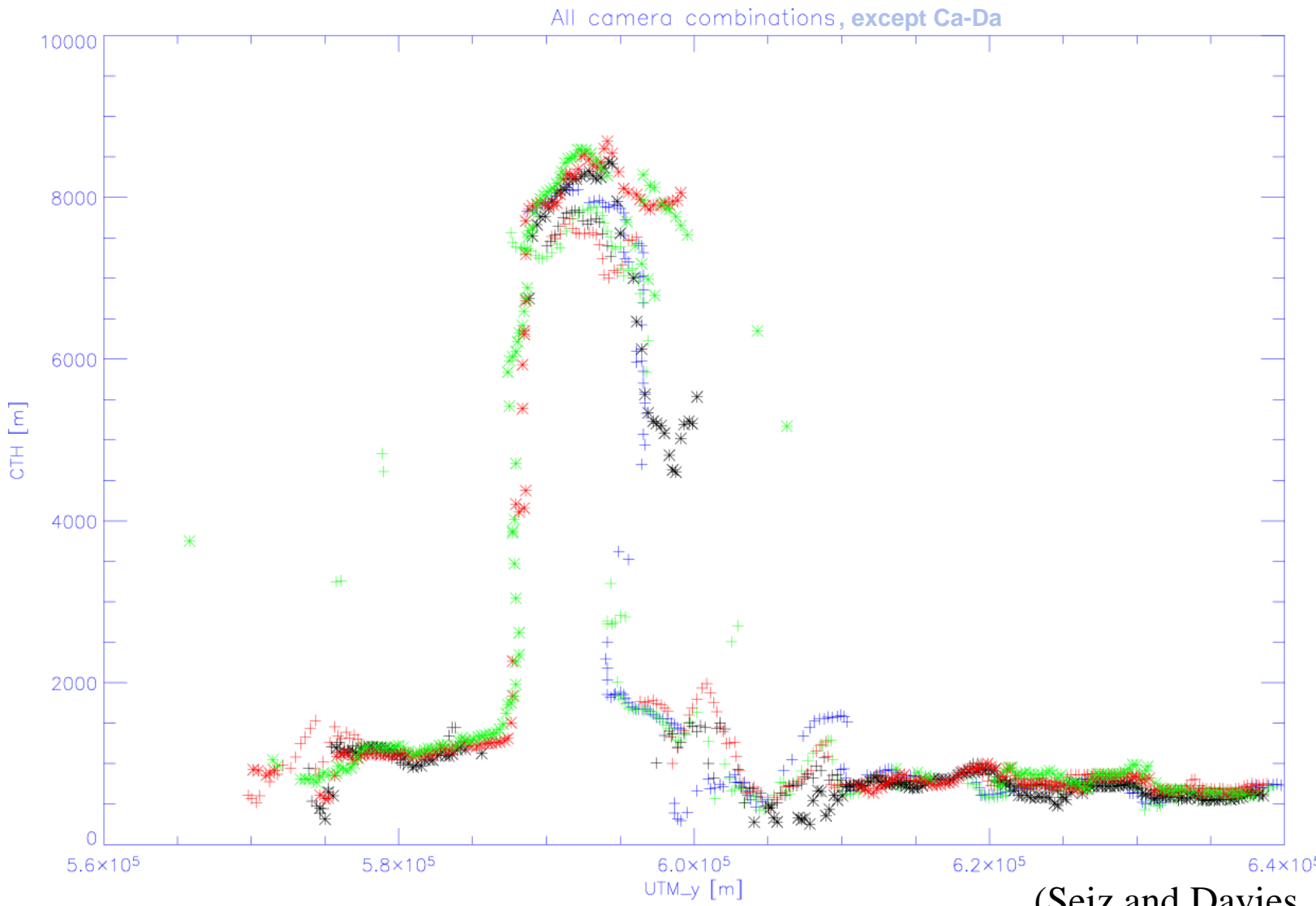


- Cf-Df

3D cloud reconstruction from MISR

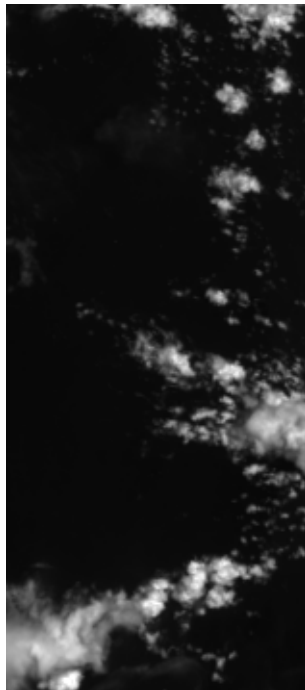
×

3D cloud reconstruction from MISR



3D cloud reconstruction from MISR

2 Sep 2003, Path

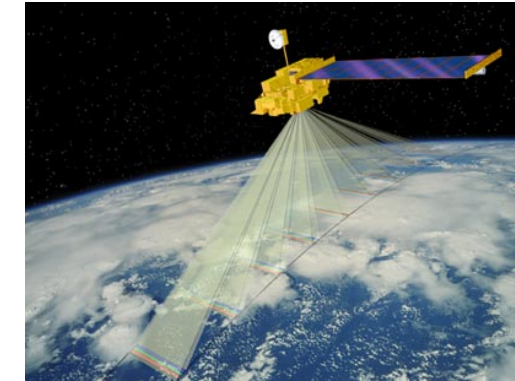


Conclusions

- Potential of stereo-photogrammetric methods on clouds
- Importance of accurate absolute and relative geolocation
- Application as independent comparison/validation data
- Potential of geostationary multi-view analysis
(→ MSG-3, MTG)
- Retrieval of high-resolution 3D cloud geometry
- Advantage of oblique viewing angles of MISR

Further examples of multi-view analysis

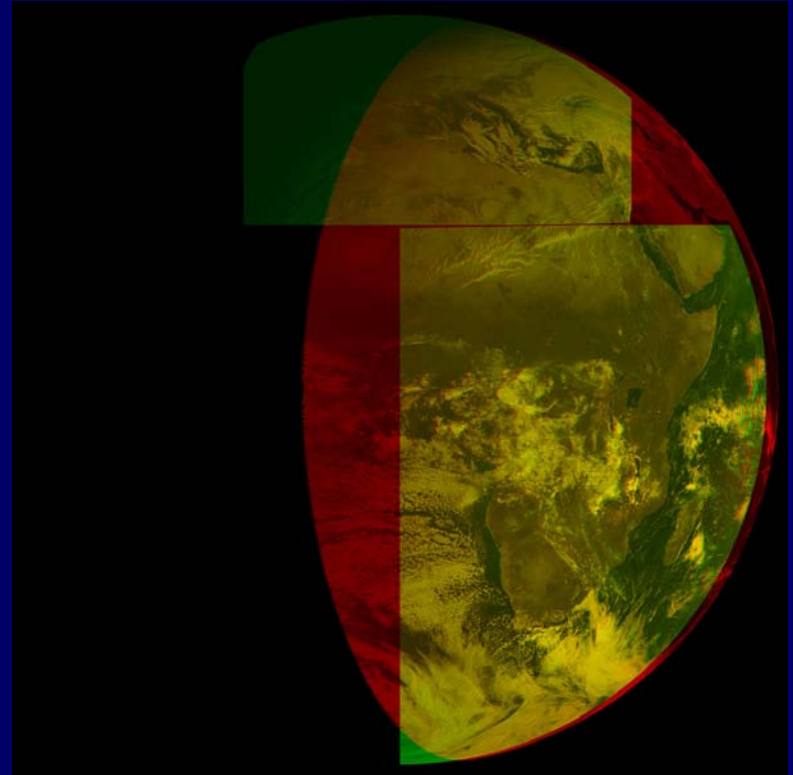
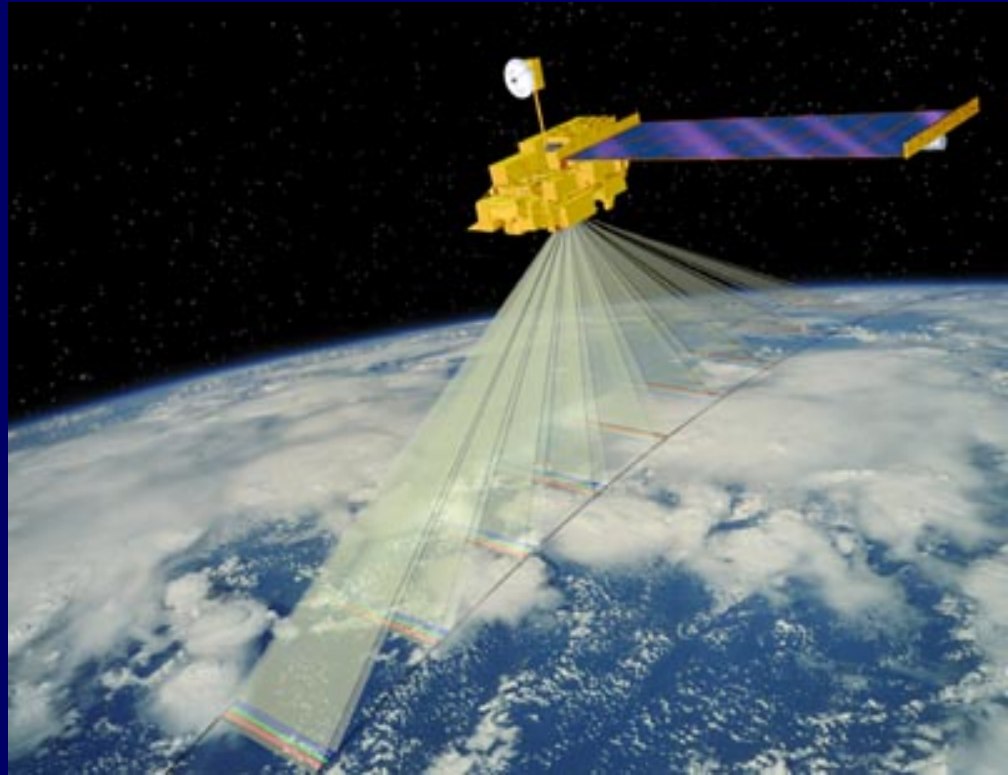
- **Aerosols**
- **Smoke plumes (volcanoes, forest fires, etc.)**
- **Cryosphere (snow, ice)**
- **Vegetation**



MISR (Courtesy: JPL)

- Diner, D., Braswell, B., Davies, R., Gobron, N., Hu, J., Jin, Y., Kahn, R., Knyazikhin, Y., Loeb, N., Muller, J.-P., Nolin, A., Pinty, B., Schaaf, C., Seiz, G., Stroeve, J. (2005). The value of multiangle measurements for retrieving structurally and radiatively consistent properties of clouds, aerosols, and surfaces. *Remote Sensing of the Environment*, 97 (4), pp. 495-518.
- <http://www-misr.jpl.nasa.gov>

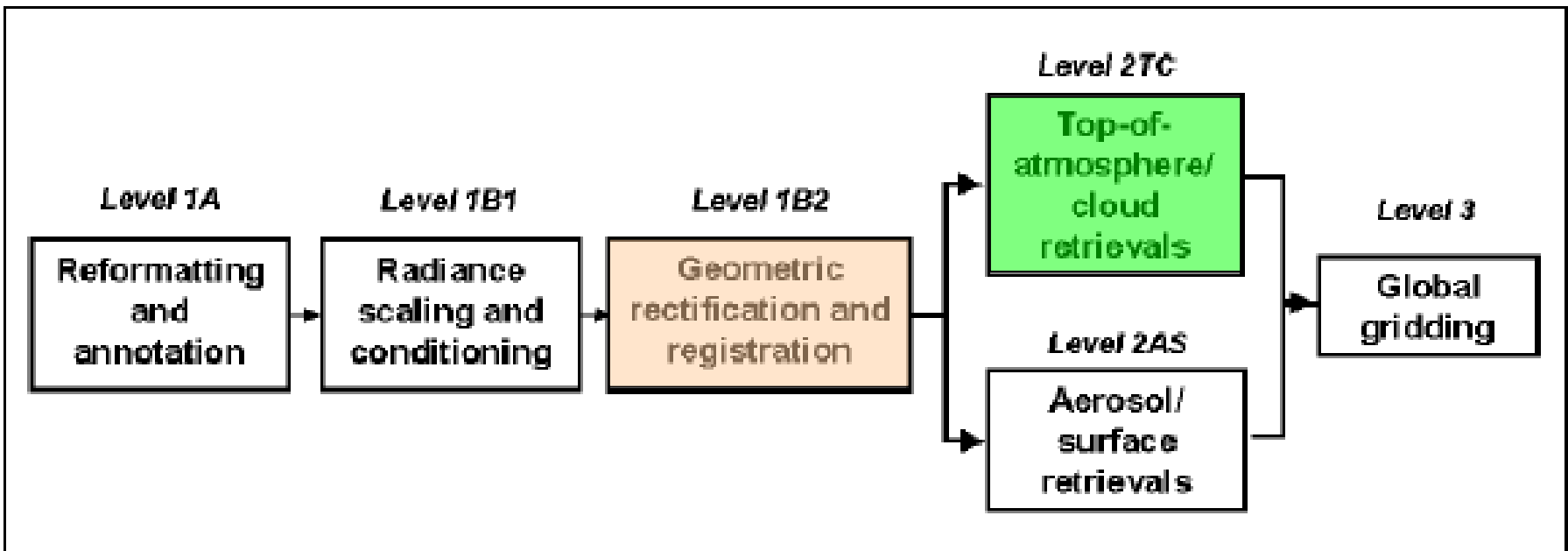
Thank you for your attention!



Dr. Gabriela Seiz

Polar-orbiting multi-view systems

- Operational stereo cloud-top height product of MISR



Case study: 28 June 2000 (Stratocumulus)

	Radio-sonde	Radar	ATSR 2				MISR	Meteosat	
Units			Stereo		Direct	OE (EUM)	OE (RAL)	Stereo	Direct
			VIS	IR					
km	2.5	2.4 ± 0.08	2.3 ± 0.2	2.6 ± 0.3	2.9	3.2	3.1	2.5 ± 0.2	3.1

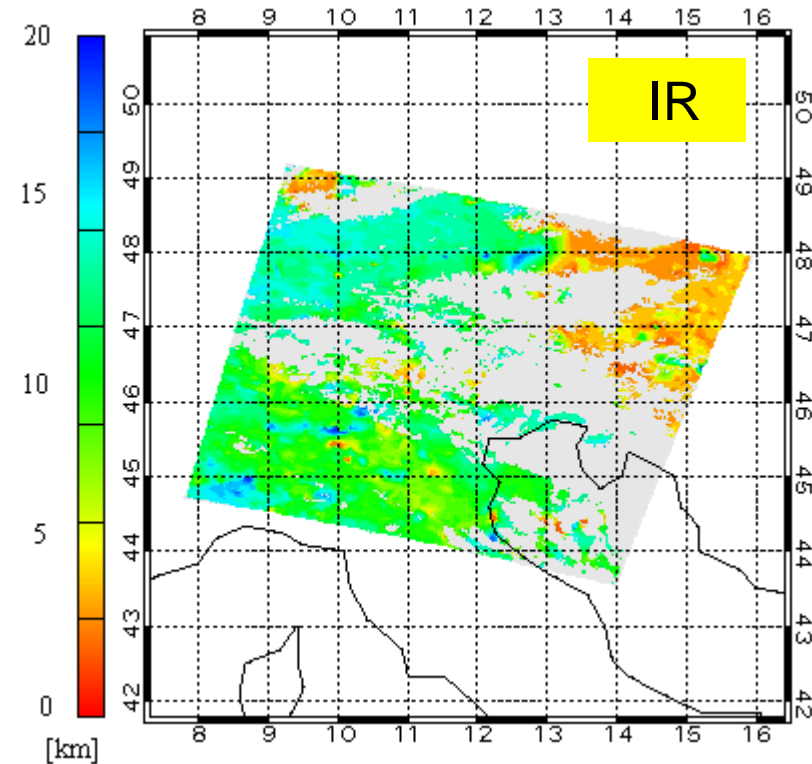
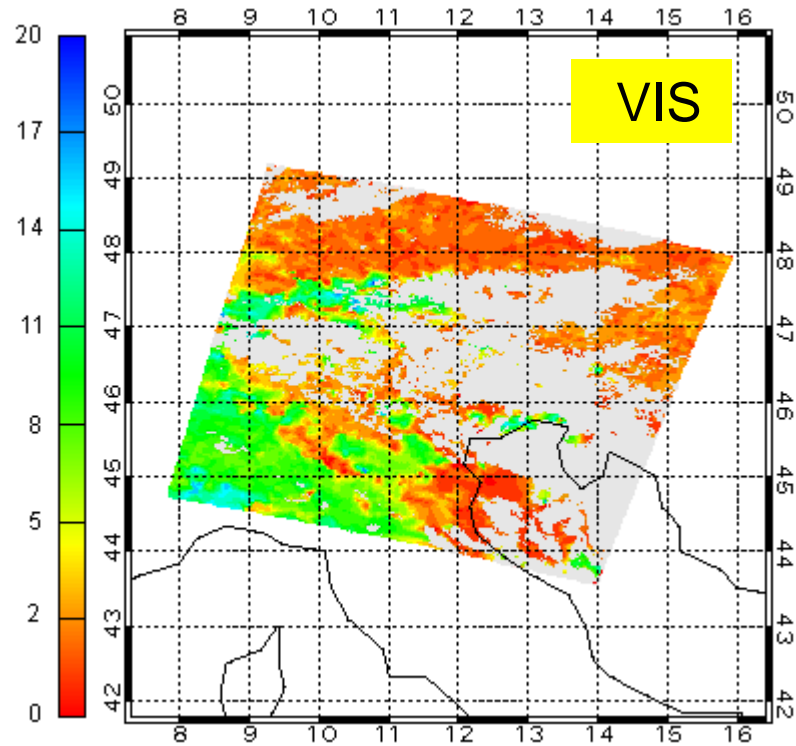
(Tjemkes et al., 2002)

Case study: 13 June 2001 (Altocumulus)

	Radio-sonde	Radar	ATSR2				MISR	Meteosat	
Units			Stereo		Direct	OE (EUM)	OE (RAL)	Stereo	Direct
			VIS	IR					
km	-	4.3 ± 0.08	-	4.5 ± 0.3	-	4.6 ± 0.6	4.5 ± 0.4	4.5 ± 0.3	-

(Tjemkes et al., 2002)

Differences between spectral channels

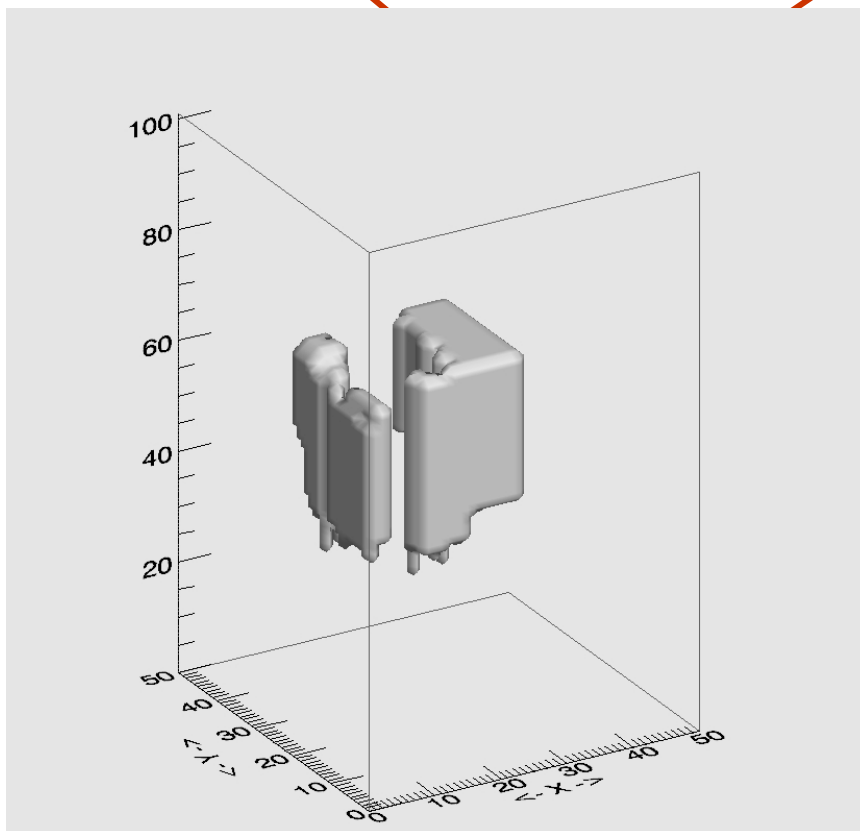


ATSR2, 13/10/1999 10:16

(Seiz, 2003)

3D cloud field data from EO and GBS

CTH field from MISR



CBH field from stereo camera system

Combined MISR + camera cloud boundaries with 3D LWC distribution (DLR)

Assimilation into very high-resolution NWP model (50 m x 50 m x 50 m aLMo at MeteoSwiss)